# Flexural-isostatic reconstruction of the Western Mediterranean during the Messinian Salinity Crisis: Implications for water level and basin connectivity

Hanneke Heida, Fadl Raad, Daniel Garcia-castellanos, Ivone Jiménez-munt, Agnès Maillard, Johanna Lofi

Received: 31 March 2021 | Revised: 23 July 2021 | Accepted: 12 August 2021

DOI: 10.1111/bre.12610

Basin Research IAS EAGE WILEY

RESEARCH ARTICLE

# Flexural-isostatic reconstruction of the Western Mediterranean during the Messinian Salinity Crisis: Implications for water level and basin connectivity

**Hanneke Heida**[1] | **Fadl Raad**[2] | **Daniel Garcia-Castellanos**[1] | **Ivone Jiménez- Munt**[1] | **Agnès Maillard**[3] | **Johanna Lofi**[2]

[1]Geosciences Barcelona (GEO3BCN-CSIC), Barcelona, Spain

[2]Géosciences Montpellier, Université de Montpellier, CNRS, Montpellier, France

[3]Géosciences Environnement Toulouse GET, OMP, Université de Toulouse, CNRS, IRD, Toulouse, France

**Correspondence**
Hanneke Heida, Geosciences Barcelona (GEO3BCN-CSIC), Barcelona, Spain.
Email: hheida@geo3bcn.csic.es

**Funding information**
GeoCAM; European Commission

## Abstract

During the Messinian Salinity Crisis (MSC, 5.97–5.33 Ma), thick evaporites were deposited in the Mediterranean Sea associated with major margin erosion. This has been interpreted by most authors as resulting from water level drop by evaporation but its timing, amplitude and variations between subbasins are poorly constrained due to uncertainty in post-Messinian vertical motions and lack of a clear time-correlation between the marginal basin and offshore records. The Balearic Promontory and surrounding basins exemplify a range of responses to this event, from margin erosion to up to a kilometre thick Messinian units in the abyssal areas containing the majority of the MSC halite. The Balearic Promontory contains unique patches of halite with thickness up to 325 m at intermediate depths that provide valuable information on water level during the stage of halite deposition. We compile seismic markers potentially indicating ancient shorelines during the drawdown phase: the first is marked by the transition from the MES to UU based on seismic data. The second is the limit between the bottom erosion surface (BES) and abyssal halite deposits. We restore these shorelines to their original depth accounting for flexural isostasy and sediment compaction. The best-fitting scenario involves a water level drop of ca. 1,100 ± 100 m for the Upper unit level and 1,500 ± 100 m for the BES level. According to our results, halite deposition began in the Central Mallorca Depression at 1,300–1,500 m depth, perched hundreds of metres above the deep basins, which were at 1,500–1,800 m (Valencia Basin) and >2,900 m (Algerian Basin). The hypothesis that erosion surfaces were formed subaerially during the drawdown phase is consistent with a model of halite deposition before/during the water level drop of at least 1,000 m, followed by the deposition of the Upper unit until the MSC is terminated by the reinstatement of normal marine conditions.

**KEYWORDS**

flexural isostasy, Messinian Salinity Crisis, paleotopography, sea-level variations, Western Mediterranean

## 1 | INTRODUCTION

The Messinian Salinity Crisis (MSC) was a period of rapid and massive environmental changes in the Mediterranean (Hsü et al., 1973) at the end of the Miocene (5.97–5.33 Ma) (Krijgsman et al., 1999; Manzi et al., 2013) leading to deposition of a layer of evaporitic sediment (mostly halite) thicker than a kilometre in the deep basins and to widespread erosion of the basin margins. Building on the model of Clauzon et al. (1996), a three-stage model of the crisis has been progressively developed (CIESM, 2008; Manzi et al., 2013; Roveri, Flecker, et al., 2014):

Stage 1 (5.97–5.60 Ma): Onset of MSC with the deposition of 'Primary Lower Gypsum' (PLG) in the marginal basins (Lugli et al., 2010) and on open continental shelves and slopes (Ochoa et al., 2015).

Stage 2 (5.60–5.55 Ma): Halite and potash salt deposition in the deep basins and local intermediate basins, for example Sicily (Lugli et al., 1999), synchronous to or followed by erosion and resedimentation of stage 1 PLG.

Stage 3 (5.55–5.33 Ma): deposition of 'Upper Evaporites' (UE) consisting of gypsum with marl interbeds with stronger freshwater input and Lago Mare event(s) (Manzi et al., 2009; Orszag-Sperber, 2006). This stage is often divided into stage 3.1 (5.55–5.42, Upper Evaporites) and stage 3.2 (5.42–5.33, Lago Mare).

The chronology and environmental conditions during the various depositional and erosional stages are still under debate. For example, some authors suggest that deep-basin halite was formed synchronously to the PLG in stage 1 in a salinity-stratified water column (Meilijson et al., 2019; Simon & Meijer, 2017; Van Ceuvering et al., 1976). Evaporite deposits in the deep basins of the Western Mediterranean have not yet been drilled beyond their topmost layer, and due to the extreme conditions during their deposition they lack biostratigraphic water depth proxies. The main evidence supporting water level variations are erosional surfaces observed in outcrops in marginal basins (Bourillot et al., 2009, 2010; Clauzon et al., 1996, 2015; Conesa & Badinot, 1999; Dabrio & Polo Camacho, 1995; Decima & Wezel, 1967; Dela Pierre et al., 2011; Do Couto et al., 2015; Dronkert, 1976; Fortuin et al., 2000; Krijgsman et al., 2001; Ott d'Estevou & Montenat, 1990; Pagnier, 1976; Riding et al., 1991; Rouchy & Saint Martin, 1992; Roveri et al., 2009; Vai & Lucchi, 1977) and in the offshore seismic record underlying, intercalated in, and on top of the Messinian deposits, pointing to a kilometric water level drop or (near) desiccation of large parts of the Mediterranean (Lofi, Déverchère, et al., 2011; Lofi et al., 2005; Lofi, Sage, et al., 2011; Maillard et al., 2006; Raad et al., 2021; Ryan, 1976; Ryan & Cita, 1978). The MSC ended abruptly with a geologically sudden reestablishment of open marine conditions, purportedly due to reflooding through the Strait of Gibraltar causing a deeply eroded channel in the Alboran basin and chaotic deposits associated with the flooding event (Blanc, 2002; Estrada et al., 2011; Garcia-Castellanos et al., 2009, 2020; Micallef et al., 2018). However, some authors have argued for much smaller water level variations (<200 m) and alternative mechanisms for the formation of incised channels (Roveri, Manzi, et al., 2014). The widespread occurrence of brackish lacustrine 'Lago Mare' deposits on top of the deep and marginal evaporites has led other authors to suggest that the basins were already connected at high water level before the end of the Messinian (Andreetto et al., 2020, 2021; Stoica et al., 2016), which would be at odds with an outburst flood from the Atlantic Ocean.

Messinian erosional surfaces and deposits have been affected by subsidence and possibly phases of rebound since the start of the MSC due to loading by sediment deposition and water level changes (Gargani, 2004; Govers et al., 2009; Norman & Chase, 1986; Ryan, 1976, 2011). Backstripping (Watts & Ryan, 1976) is a classical technique used to calculate the isostatic and compaction effects due to sediment loading. Traditionally,

**Highlights**

- Restored topography during the Messinian Salinity Crisis, including and excluding effects of a large water level drop.
- Water level estimates from restored elevation of potential paleoshoreline markers at −1,500 m for the bottom erosion surface, and −1,100 m for the Upper unit deposition.
- Halite was deposited or preserved in local topographic minima at various depths on the Balearic Promontory, their thickness being controlled by the depth of such depressions.

this technique has been used to constrain the vertical motions related to tectonic loading by thrusting or extension, provided the availability of precise paleobathymetric measures. However, in areas where tectonic loading is negligible, it can a priori be inverted to constrain paleobathymetry (Amadori et al., 2018). The technique has been applied to constrain the original depth of the Messinian units and erosional surfaces in wells and along sections in the Gulf of Lions (Ryan, 1976), the Tertiary Piedmont Basin (Amadori et al., 2018), the Balearic Promontory (Mas et al., 2018), and in the Ebro delta (Urgeles et al., 2011). This has led to drawdown estimates in the Western Mediterranean of 1,300 m of late-Messinian water level drop based on terrace formation in a fluvial erosion network (Urgeles et al., 2011) and a minimum of 800 m drawdown to facilitate faunal colonisation of the Balearic Islands (Mas et al., 2018).

Except for Amadori et al. (2018), the aforementioned studies have been based on either local isostasy or 1D (cross-section) flexural isostasy. Although a 2D (planform or pseudo-3D) technique was used by Govers (2009) and Govers et al. (2009), these studies were not designed to reconstruct the pre-MSC bathymetry nor reconstruct the shoreline positions. For this reason, paleobathymetric reconstructions based on erosional/depositional markers are only locally available in specific areas of the Western Mediterranean and their consistency is difficult to evaluate.

In this paper, we aim at using a 2D (planform, pseudo-3D) flexural backstripping technique supported by an extensive set of seismic data to quantify Messinian and post-Messinian vertical motions and constrain the paleodepth and the magnitude of the Messinian water level drop at the scale of the Western Mediterranean. To this purpose, we constrain the model with paleoshoreline indicators from the seismic record. The starting hypothesis of our study is therefore that these stratigraphic features were formed near the shore during the MSC. The depth range of the Valencia Basin and Balearic Promontory and their unique distribution of Messinian markers (Figure 2) with erosion on the margins (Cameselle & Urgeles, 2017; Driussi et al., 2015; Maillard et al., 2006, 2014; Urgeles et al., 2011), Upper unit in the Valencia Basin (Maillard et al., 2006) and a complete MSC trilogy in the deep basin (Figure 2a; Lofi, Déverchère, et al., 2011; Lofi, Sage, et al., 2011) provide an opportunity to constrain the progression of water level during the MSC in a region that covers the gap between shallow evaporite deposits (primary gypsum) and the deep (abyssal) salt deposits visible in the seismic record. A compilation of key MSC-related features including evaporite deposits and erosional surfaces is presented in Figure 1.

## 2 | GEODYNAMIC SETTING

### 2.1 | Tectonic setting

The Western Mediterranean comprises basins with distinct ages, tectonic styles and crustal nature. They formed as back-arc basins due to slab rollback of the retreating Apennines subduction in a general setting of N–S convergence between the African and Eurasian plates since the Miocene (Faccenna et al., 2004; Gelabert et al., 2002; Gueguen et al., 1998; Jolivet et al., 2006; Malinverno & Ryan, 1986; Martínez-Martínez & Azañón, 1997; Mauffret et al., 1995, 2004; Schettino & Turco, 2006).

The Neogene Valencia Basin is a region of continental crust which was extended between 28 and 10 Ma (Bartrina et al., 1992; Etheve et al., 2018; Roca & Guimerà, 1992; Watts & Torné, 1992a), bounded by the Iberian Margin to the northwest and the Balearic Promontory to the southeast. To the east, the Valencia Basin is bounded by the North Balearic Fracture Zone (Galdeano & Rossignol, 1977; Maillard, Jolivet, et al., 2020; Rehault et al., 1984) which accommodated the anticlockwise rotation of the Corsica-Sardinia-Calabria blocks with the emplacement of the oceanic crust of the Provençal basin between 22 and 16 Ma (Alvarez, 1972; Burrus, 1984; Gueguen et al., 1998; Speranza et al., 2002). Contrary to the Provençal Basin, the Valencia Basin extension did not attain the formation of oceanic crust. Instead, extension jumped to the southern side of the easternmost Betic range to form the Balearic promontory and open the Algerian Basin.

The Algerian Basin opening in the Miocene (16–8 Ma) has long been thought to be the result of the westward migration of the Alboran block due to rollback of the subducting Tethys plate (Lonergan & White, 1997; Rosenbaum et al., 2002). However, recent alternative models suggest that it can also be explained by back-arc spreading during the southwards retreat of the neotethyan subducted slabs (Faccenna et al., 2004; Vergés & Sàbat, 1999), ending before 8 Ma. It is separated from the Balearic Promontory by the Emile Baudot and Mazzaron Escarpments, structures that have been proposed to be the remnants of a transfer fault along which the Alboran domain migrated westward (Acosta et al., 2001; Mauffret et al., 2004).

With the exception of the Tyrrhenian Basin, all Western Mediterranean basins were formed before the onset of the MSC (Ryan, 1976). The present-day thickness variations of the MSC units are therefore thought to be related to paleo-waterdepth and post-Messinian vertical movements (e.g. Lofi, Sage, et al., 2011). Thin-skinned salt tectonics and subsequent deformation of the salt (diapirism) is another cause for the present-day thickness variation (CIESM, 2008; Dal Cin et al., 2016). Recent shortening has been reported between Alicante and Ibiza (Maillard &

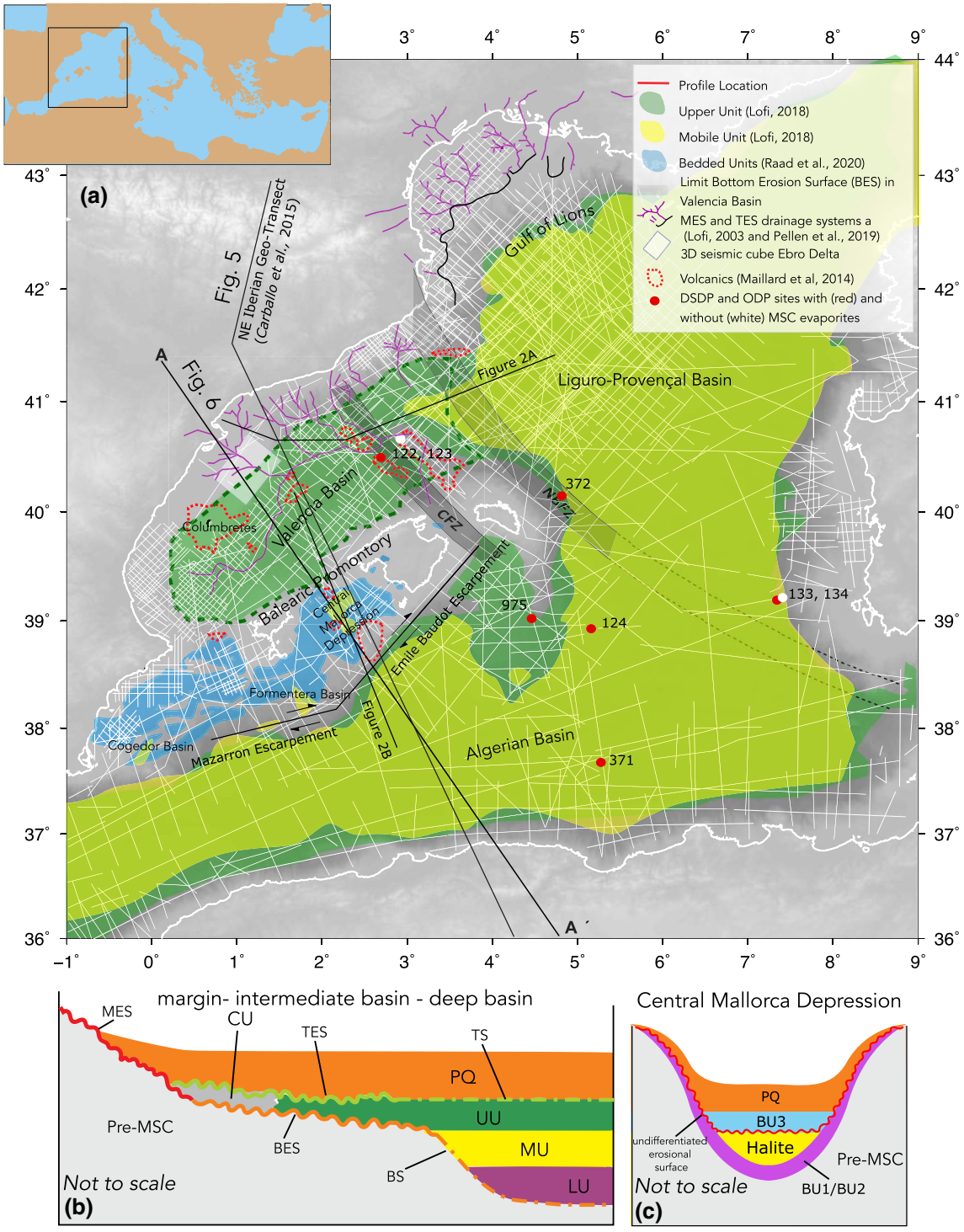


**FIGURE 1** (a) Topographic map of the Western Mediterranean area with the distribution of the main Messinian deposits and erosional features. It includes the main tectonic structures and locations of DSDP boreholes, seismic data used in this study (thin white lines), and location of the representative seismic profiles (Figure 2) used for lithosphere characterisation (Figure 5) and the backstripping restoration (Figure 6). CFZ: Catalan Fracture Zone; NBFZ: North Balearic Fracture Zone. (b) Schematic cross section of the Western Mediterranean basin illustrating the present day distribution of sedimentary units and surfaces after Lofi (2018). (c) Schematic cross section of the Central Mallorca Depression (post) Messinian units (BU = Bedded unit) and surfaces

Mauffret, 2013), and post-MSC tectonics has also been reported on Mallorca Island and in the CMD, interpreted in relation with strike-slip movements located in WSW-ENE narrow depressions. As this deformation affects the MSC markers only locally, so we do not consider this deformation in our basinwide reconstruction.

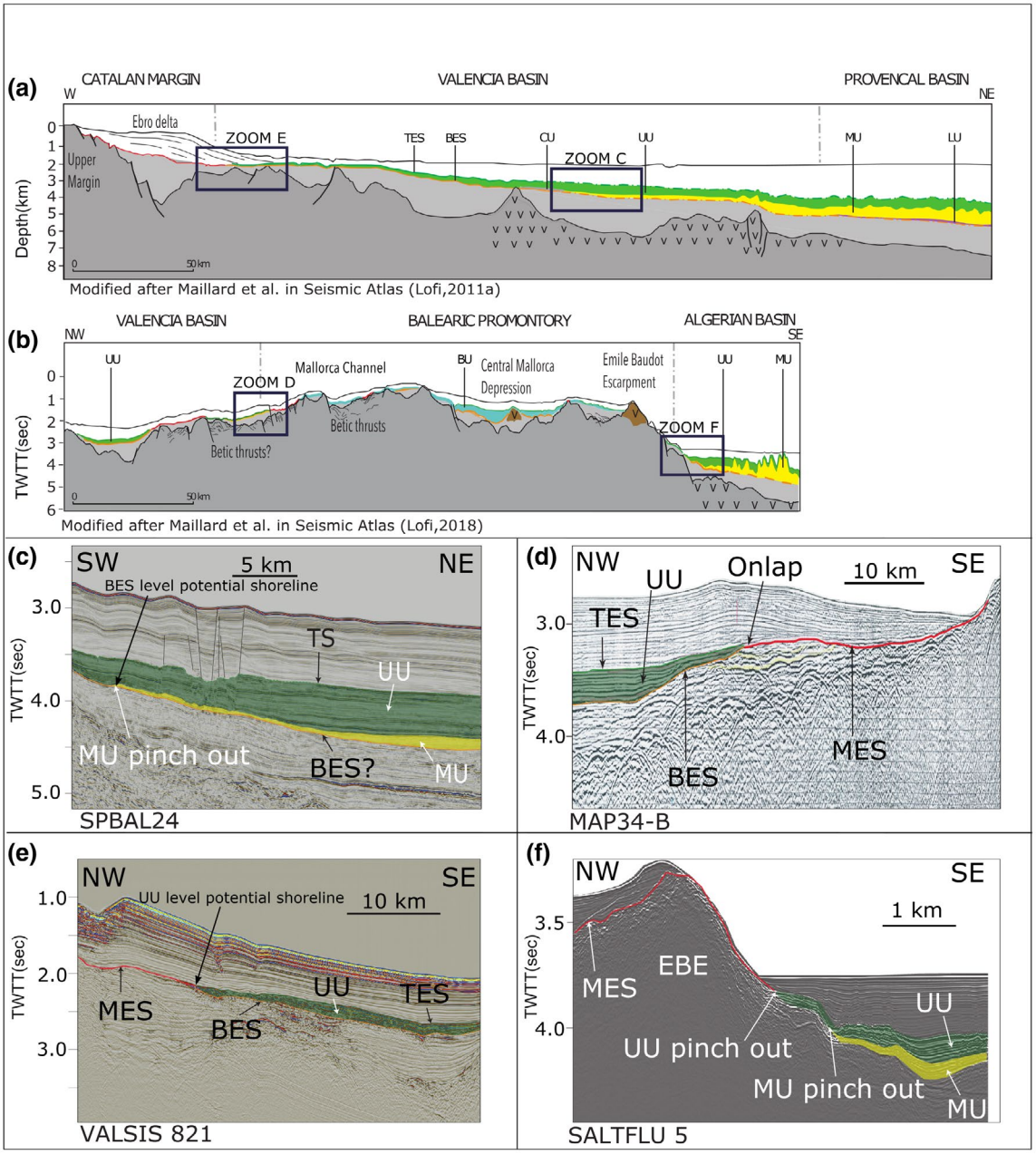


**FIGURE 2** (a and b) Line drawing composite profiles crossing key structural and sedimentary domains in the Western Mediterranean (from seismic atlases, Lofi, Déverchère, et al., 2011, 2018), position of profiles in Figure 1. (c–f) Representative seismic lines with interpreted erosional features and MSC related evaporite units. (d) Modified after Maillard et al. in Lofi, Déverchère, et al. (2011). (f) Modified after Camerlenghi et al. in Lofi, Déverchère, et al. (2011)

## 2.2 | Volcanism

Two distinct volcanic phases have been identified in the Western Mediterranean (Maillard et al., 1992; Martí et al., 1992). The first, mostly represented by calc-alkaline affinity, has been related to the emplacement of a volcanic arc of the SE-retreating subduction also observed in Sardinia, Corsica and Ligurian domains and is coeval to the Valencia rifting stage (Late Oligocene–Early Miocene age), whereas the second stage is alkaline and represented by the Columbretes and the Southwest Mallorca Field on the Emile Baudot Escarpment (Late Miocene–Recent), and could be linked to regional decompression during extension (Acosta et al., 2001, 2004; Martí et al., 1992; Réhault et al., 2012). This recent volcanism locally deformed the MSC deposits and erosion surface. The large extent of the volcanoes in the Valencia Basin surely affected the thermal history of the basin. Based on well data from the Catalan margin, these volcanic phases have been proposed to have counteracted general subsidence due to

relaxation after the end of the main rifting phase at 10 Ma in the Valencia Basin (Watts & Torné, 1992).

## 2.3 | Messinian Salinity Crisis (MSC) stratigraphy

The distribution of the MSC sedimentary sequences is used to define paleoshoreline indicators that constrain our model. They have been identified and widely studied and described mainly from seismic datasets by several authors (Camerlenghi et al., 2009; Cameselle & Urgeles, 2017; Dal Cin et al., 2016; Driussi et al., 2015; Lofi, Sage, et al., 2011; Maillard et al., 2006; Ochoa et al., 2015; Urgeles et al., 2011; Lofi, 2018 and references therein; Pellen et al., 2019; Raad et al., 2021).

The deep basins of the Western Mediterranean (i.e. Provençal and Algerian Basins) contain the full MSC trilogy (e.g. Lofi, Sage, et al., 2011 see also Figure 1b), identified mainly through seismic reflection profiles with its components listed below:

- Lower unit (LU): age, origin and lithology remain unclear. It has been suggested to be a shale equivalent to stage 1 PLG (Manzi et al., 2007, 2018).
- Mobile unit (MU): here considered representative of 'stage 2' lies conformably above the LU in the deep basins. Towards the limits with the intermediate depths (i.e. Valencia Basin), MU lies above pre-MSC sediment along a bottom erosion surface (BES) or Bottom Surface (BS) where conformable (Figure 2a,c). Its upper boundary is conformable. The MU consist of up to a kilometre-thick transparent seismic facies that is thought to contain mainly halite and is highly deformed by salt tectonics. It pinches out everywhere on the borders of the deep basins (Figure 2a–c,f).
- Upper unit (UU): deposited during 'stage 3' lies conformably above the MU in the deep basins, whereas towards the intermediate depths beyond the extent of MU it lies above the BS/BES. In the deep basins, the upper boundary of the UU is conformable with the overlying PQ unit (TS), whereas in the intermediate Valencia Basin it is cut by a top erosion surface (TES) (Figure 2a,d,e). The uppermost part of the UU has been drilled, and it is made of alternations of gypsum and clastic deposits (ODP initial reports volume 161; Ryan, 2009). Its thickness reaches ca. 1,000 m in the deep basins (Figure 2c; Lofi, Sage, et al., 2011), where it pinches out towards the slopes (Figure 2b,f). In the Valencia Basin, the UU thins gradually from 500 m thickness (Figure 2d,e) pinching out towards the Catalan and Ebro margins. Here the Bottom and Top Erosion Surfaces bounding the UU merge into the polygenic Margin Erosion Surface (MES).

Several interpretations in terms of water level change exist to account for the observed geometries and extent of erosional surfaces. We briefly describe those interpretations and present the scenario we adopt to test in our model. The depositional environment for the Lower unit is hard to constrain, as its lithology is not known beyond its seismic reflectivity. There are no indications of water level variations during the deposition of this unit, and therefore we do not consider it as a separate stage in our topographic restoration. It is evident from well data in the Alboran Basin that restriction of the Atlantic-Mediterranean connection started affecting the depositional environment at ca. 7.2 Ma, well before the onset of evaporite deposition (Bulian et al., 2021).

A water level drop leading to margin erosion occurred after deposition of the PLG in the marginal basins (Krijgsman et al., 1999) and the MU precipitated from a brine formed under conditions of restricted, but probable continuous connectivity to the Atlantic. MU deposition possibly started before and surely continued during the stage of water level drop, but without the supply of marine waters from the Atlantic cannot have continued throughout a prolonged lowstand. Evidence for a change of deep brine precipitates to playa lake facies inside the halite unit is found in the Realmonte salt mine in Sicily (Lugli et al., 1999) although this might not be representative for the deep basin deposits. The amplitude of the water level fall is controversial, as it varies between a few hundred metres for some authors (Roveri, Flecker, et al., 2014 and references therein, Roveri, Manzi, et al., 2014) and more than one kilometre for others (Lofi, Sage, et al., 2011). Maillard et al. (2006) believe that it is during this kilometre amplitude water level drawdown that the BES was formed, due to subaerial exposure of the entire Valencia Basin.

Most authors believe that the emplacement of the UU happened during a rise in water level during the final MSC stage, causing its aggrading and onlapping geometry (Lofi, Déverchère, et al., 2011; Lofi, Sage, et al., 2011). The onlaps of the UU are interpreted as indicators of successive paleoshorelines (Lofi et al., 2005).

For some authors, the nature of the TES in the Valencia Basin could be a result of dilution during the Lago-Mare phase, and/or subaerial exposure preceding the Zanclean reflooding (Escutia & Maldonado, 1992; Maillard et al., 2006). For others, this erosion is minor and can be found only locally due to the dilution during the Lago Mare event (Cameselle & Urgeles, 2017). A significant water level drop in Valencia Basin with unclear timing and magnitude is agreed upon (Cameselle & Urgeles, 2017; Cameselle et al., 2014; Maillard et al., 2006; Urgeles et al., 2011).

In the southwestern Valencia Basin, Cameselle and Urgeles (2017) identified a widespread Complex

unit locally overlain unconformably by a thin UU. The Complex unit is interpreted here as a mass transport deposit resulting from the destabilisation of the slope during the first Messinian lowstand exposing the shelf and upper slope. Complex units with different origin and timing are also present at the downslope mouth of Messinian valleys (Lofi et al., 2005; Maillard et al., 2006) and especially in the Gulf of Lions (Lofi et al., 2005).

On the Balearic Promontory, recent studies show the presence of widespread bedded units (Bedded unit) and relatively thin salt patches (Driussi et al., 2015; Maillard et al., 2014; Raad et al., 2021). These units seem to be discontinuous between the Balearic Promontory and the surrounding deeper basins.

Raad et al. (2021) interpreted the MSC units of the Central Mallorca Depression as an undeformed analog of the Sicilian MSC records. They recognised the equivalent of the PLG, salt and Upper Evaporites (UE). These authors suggest that the CMD was disconnected from the surrounding deep basins during the MSC water level fall. They identify a prominent erosional surface cutting the top of the PLG and of a salt unit in the depocenter (Figure 1c). This surface lies at a present-day depth of ca. 1,550 m below sea level (Figure 2b), and is interpreted as the result of exposure or dissolution of salt in shallow water.

On Mallorca and Ibiza, the MSC record is mainly expressed by the terminal carbonate complex lying today between 30 and 60 m above sea level (Maillard, Gaullier, et al., 2020; Mas & Fornós, 2011). It is thought that the terminal carbonate complex formed close to sea level, starting from stage 1 of the MSC contemporaneous to the PLG (Cornée et al., 2004; Mas & Fornós, 2013; Roveri et al., 2009). Onshore drillings in the Palma de Mallorca basin also evidenced the presence of stage 1 PLG (García-Veigas et al., 2018; Rosell et al., 1998) lying below the PQ sediment, only a few tens of metres below sea level. Local water level recorded by phreatic overgrowths on speleothems in caves on the SE coast of Mallorca were recently established to have been at 33.3 and 31.8 m above modern just before and during stage 1 of the MSC respectively (Dumitru et al., 2021), although these were not corrected for vertical motions induced which the authors point out is necessary to properly interpret these water level results.

## 3 | DATA AND METHODS

### 3.1 | Paleoshoreline markers and tested scenarios

In this study, we constrain vertical motions and bathymetric changes during and after the MSC using pseudo-3D flexural-isostatic backstripping. We consider scenarios with and without a water level fall and investigate their implications for Mediterranean bathymetry, constraining the original depth of the proposed paleoshoreline markers. The first scenario relies on those by Maillard et al. (2006), Ryan (2009) and Lofi, Sage, et al. (2011) which propose the following MSC seismic markers as potential paleoshorelines during the MSC:

- The onlap of UU onto the margins is considered the main paleoshoreline indicator towards the end of the MSC, where the MES splits into BES and TES bracketing Messinian deposits. The deposition of UU is proposed to occur in shallow waters (Cameselle & Urgeles, 2017; Cameselle et al., 2014; Lofi et al., 2005; Maillard et al., 2006), before a rapid reflooding (Garcia-Castellanos et al., 2020 and references therein). The onlap of the top of the UU on the MES likely represents the highest water level during its deposition, although the top of the UU shows truncations (TES) that indicate possible variations around this water level. This stage is referred to as the UU level.
- The limit of the BES to MU on the margins is hypothesised to be another indicator of the paleo-shoreline after salt emplacement following an evaporative drawdown (Ryan, 2009). During this lowstand, the BES developed in the Valencia Basin, where almost the entire region was subaerially exposed (Maillard et al., 2006). The elevation of the MU limit is variable due to the extensive erosion/dissolution that affected it after deposition. The shallowest preservation of halite limits the BES, and is therefore our reference point. The limit was also affected by halokinetic activity (Badji et al., 2015; Dal Cin et al., 2016). However, the distal limit of the imaged BES offers a constraint on the minimum amount of water level drop required to expose this region, although water level might have been lower, as a constraint on the maximum water level drop is not available. We therefore refer to this shoreline marker as the BES level.

The second tested scenario assumes no significant base-level change, maintaining a deep Mediterranean basin throughout the formation of evaporites and erosional surfaces. We present the bathymetric implications of this scenario during the MSC compared to a scenario with considerable drawdown.

### 3.2 | Flexural-isostatic backstripping

Pseudo-3D (planform) flexural-isostatic modelling of vertical motions due to surface loading was performed using TISC software (Garcia-Castellanos et al., 2002) allowing for

a basin-wide evaluation of the topographic evolution during the MSC. The current basin state with the depth of bounding surfaces and the thickness of the various stratigraphic units is defined in grids of 200 × 200 resolution spanning an area of 860 by 890 km corresponding to the area in Figure 1. We perform backstripping accounting for the subsidence caused by sedimentation and rebound due to the removal of a water load during periods of low water level, as well as compaction of the pre-Messinian sediment unit (Figure 3). The flexural calculations adopt an elastic thin plate, assuming that loads are supported only by a strong lithosphere laying on a low-viscosity asthenosphere which behaves like a fluid. This approach does not allow for the evaluation of the initial time-dependent (transient) response to loading, which is rapid (10–30 kyrs) compared to the geological processes we study here, which is why an equilibrium state for the basin is a valid assumption in most circumstances. Figure 3 illustrates the workflow and method for matching paleoshoreline positions to modelling results.

The effective elastic thickness (EET) of the lithosphere controls the magnitude of vertical motions as a response to tectonic and sedimentary loads (Burov & Diament, 1995; Watts, 2001), and is a crucial input parameter for flexural-isostatic modelling. For continental lithosphere, EET values are related to the thermal state (high geothermal gradients due to recent extension causing lower EET) and the state of the crust-mantle interface. *Decoupling*, meaning the existence of a low-strength zone between the lower crust and upper mantle, prevents an applied load force from being transferred to and supported by the upper mantle. This reduces the EET value to solely that of the crust. In addition, the local curvature of the plate inducing bending stresses can weaken the plate (Burov & Diament, 1995).

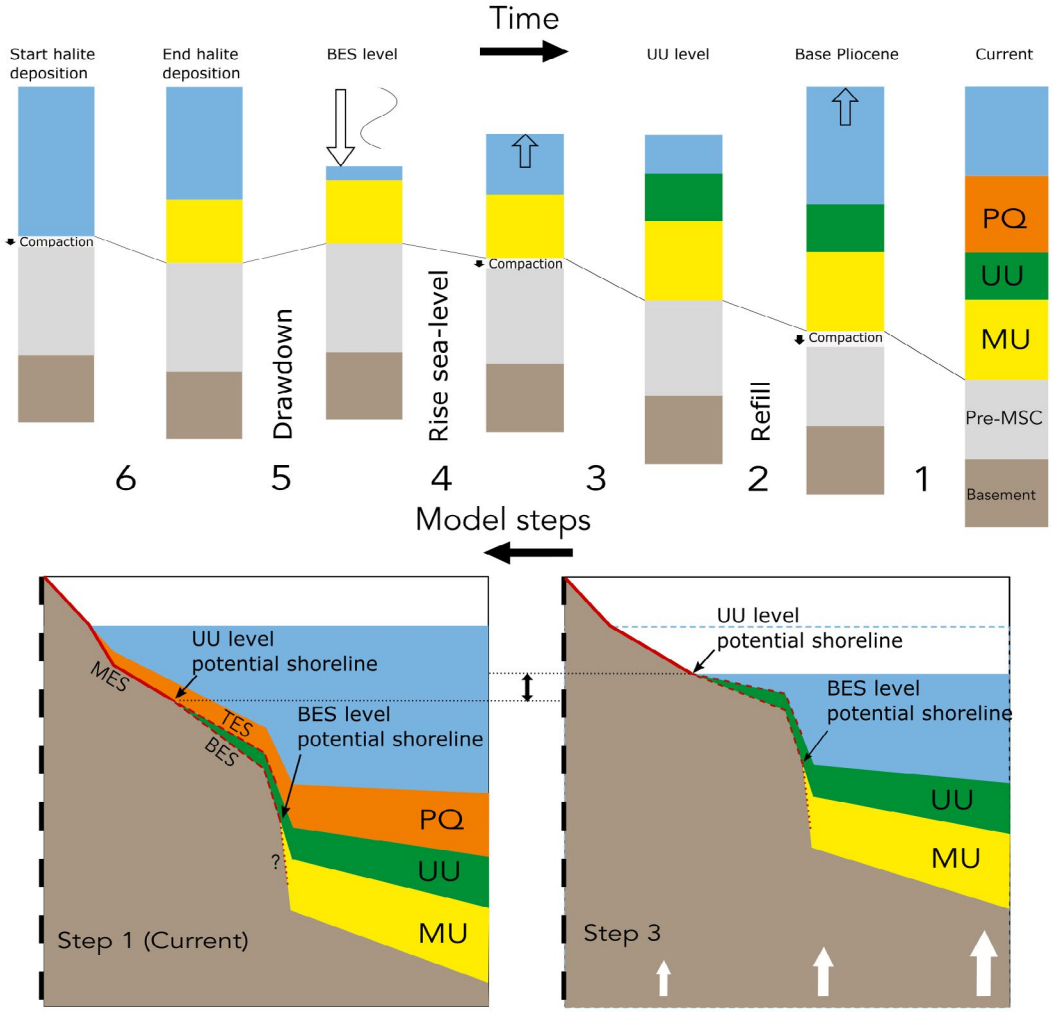


**FIGURE 3** Schematic cross section showing step-by-step backstripping of sediment and water to determine flexural-isostatic response and match water level to paleoshorelines. 1: Removal of Plio-Quaternary sediment 2: Restoration of water level to pre-Zanclean flood level (UU lowstand) 3: Removal of UU sediment 4: Lowering of water level to lowest level at 'acme' (BES lowstand) 5: Restoration of water level to pre-drawdown level 6: Removal of MU halite, to obtain bathymetry before the onset of stage 2 of the Messinian Salinity Crisis

We first estimate EET values from the Yield Strength Envelopes of the lithosphere obtained from thermal and structural information (Figure 5). Geotherms were calculated for the main domains along the NE Iberian Geo-Transect (Carballo et al., 2015, see Figure 1 for location), using MOHO and LAB depth, surface heat flow, average crustal and mantle compositions, crustal radiogenic heat production and average thermal conductivity. We test for a range of lithospheric strength parameters by using activation energy values from Govers and Wortel (1995) and Cloetingh and Burov (1996). Using the tAo code (Garcia-Castellanos et al., 1997) we calculate the effect of curvature due to sediment loading along a 2-D profile crossing the main crustal blocks (Figure 6, see Figure 1 for position profile A).

Bathymetry of the target region was derived from the GEBCO_2014 (IOC-IHO) grid. The thickness of the offshore Miocene to Quaternary deposits in the Western

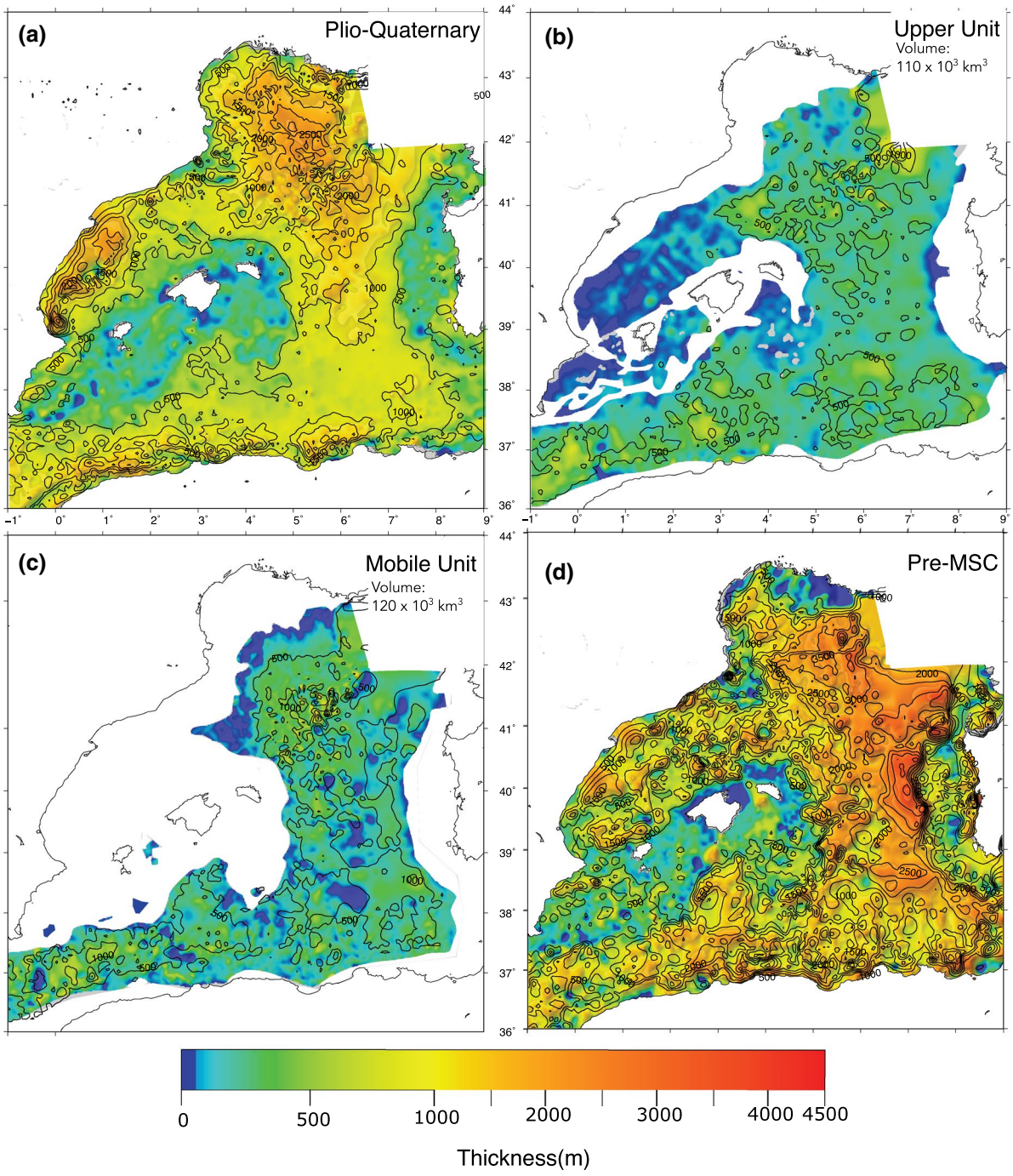


**FIGURE 4** Thickness in metres of sedimentary units used in the reconstruction, as interpolated from the seismic dataset compilation in Figure 1, using velocities presented in Table 1

Mediterranean (Figure 4) was determined from compilations of extensive seismic surveys (Figure 1) including partially reinterpreted 2D seismic lines (Acosta et al., 2001; Gallart et al., 1995; Just et al., 2011; Leroux et al., 2019; Maillard & Mauffret, 1993; Maillard et al., 1992, 2014; Mauffret et al., 1995; Raad et al., 2021; Roca & Guimerà, 1992; Sàbat et al., 1997) and a 3D cube in the Ebro delta region (Urgeles et al., 2011). The seismic derived bathymetry, base PQ and the acoustic basement are available online as part of a wider dataset in the Western Mediterranean (Bellucci et al., 2021).

Although some sediments were deposited onshore their limited thickness and lateral distribution make for small effects when considering the regional scale, so we limit our investigation to offshore regions. In the northeastern corner of our region data was not available, so grids were extended manually to be consistent with the deep basin thicknesses and prevent artefact shorelines in the Ligurian and Provençal basins. The reconstruction east of the Gulf of Lions and north of Corsica is therefore not accurate. The thickness of the MU (Figure 4c) is locally higher in the Provençal basin (reaching up to 2 km) due to the presence of diapirs deforming the overlying UU (Figure 4b) and Plio-Quaternary (Figure 4a) units. The volumes of the MU and UU in our study area are $0.11 \times 10^6$ and $0.12 \times 10^6$ km$^3$ respectively, summing to $0.23 \times 10^6$ km$^3$. This is considerably lower than older estimates ($0.5 \times 10^6$ km$^3$, Ryan, 2008) and still considerably lower than the $0.33 \times 10^6$ km$^3$ reported by Haq et al. (2020), but this can be due to the fact that volume from Haq et al. (2020) also includes the Lower unit evaporites in the Western Mediterranean.

It should be noted that the distribution of the earliest sediment associated by some authors with the MSC (Lower unit or LU) is not included in this reconstruction. No age control exists for the deep MSC record in the Western Mediterranean and some authors question its age and origin (e.g. Raad et al., 2021). Moreover, the passage from pre-MSC sediment to evaporitic facies marking the onset of the MSC has been proven to be conformable all around the Mediterranean with no evidence of water level drop at this stage (Dela Pierre et al., 2011; Lugli et al., 2010; Ochoa et al., 2015). Therefore, unlike Bache et al. (2009) and Haq et al. (2020), we incorporate the LU in the pre-MSC sediment (Figure 4d).

On the Balearic Islands we estimate the magnitude of post-MSC erosion by distributing the volume of clastic sediment in the Plio-Quaternary deposits on the offshore promontory onto the currently exposed surface area of the Balearic Islands (see Appendix B), assuming the same area of subaerial exposure as in the modern day (the sum of the islands area is 4,907 km$^2$) and a range of 30%–70% for clastic provenance of sediment as found in the post-Messinian unit I in ODP borehole 975 (Comas et al., 1996). This rough estimate allows us to describe the changes in surface topography since the MSC as well as the flexural-isostatic effect of this erosion. The onshore PQ sediment in the Palma graben (Capó & Garcia, 2019) is not considered as this was only transported over short distances, mostly sourced from the northwestern Tramontana range and therefore had a negligible regional isostatic effect.

The full Messinian succession in the deep basin has not been drilled, which means it lacks a definitive constraint on density and other petrophysical characteristics required to convert the travel time of seismic waves to the key horizons to depth and determine the mass of the sediment and evaporite loads. Well data provide constraints for the top of the sequence, and we can assume a degree of similarity with the evaporite record found onshore. For the Pliocene-Quaternary sequence, we assume a velocity function proposed by Urgeles et al. (2011) based on calibration from FORNAX-I well data on the Ebro margin. It takes the form:

$$\text{depth [m]} = 1135.1 \times \text{TWTT [s]}^{1.343}$$

The UU is assumed to consist of intercalated gypsum/anhydrite and clays (Ryan, 2009), similar to the cycles observed in marginal basins which are proposed to have resulted from climate variations by precession cycles (Dronkert, 1985; Manzi et al., 2009). The MU, similar to the succession found in the Realmonte mine in Sicily is thought to consist of almost pure halite and potash salts (Lugli et al., 1999; Samperi et al., 2020), as evidenced by its seismic facies and the widespread halokinetic activity (Gaullier et al., 2008). Velocities and densities used in assessing our load distributions are listed in Table 1.

From these densities, we can derive the ratio of a response under *local isostasy* between the load thickness and induced subsidence or rebound for each step (see Appendix A).

**TABLE 1** Average seismic velocities and densities used for each unit

| Unit | Water | Plio-Quaternary | Upper unit | Mobile unit | Pre-halite |
|---|---|---|---|---|---|
| Av. seismic velocity (m/s) | 1,500 | Power law (see text) | 3,400 | 4,800 | 2,440 |
| Av. density (kg/m$^3$) | 1,030 | 2,100 | 2,500 | 2,170 | 2,700 |

For long-wavelength and uniform loads, such as those in the deep Mediterranean basins the response will be close to local isostasy (see Appendix A), but for more variable loads and close to load edges the response will be affected by the load-bearing capacity of the lithosphere.

The effect of compaction on the pre-halite bathymetry is determined for compaction following the standard porosity-depth relationship: $\phi_z = \phi_0 \times e^{-bz}$,where $\phi$ is porosity, $z$ is depth below seafloor (km) and b is the compaction coefficient ($km^{-1}$), for shale $\phi_0 = 0.67$, $b = 0.00051$, and for sand $\phi_0 = 0.49$, $b = 0.00027$ (Sclater & Christie, 1980). Bessis (1986) presents a porosity-depth curve based on three wells in the Gulf of Lions which fits a relationship of $\phi_0 = 0.75$ and $b = 0.00115$, suggesting slightly faster compaction than the shale curve from Sclater and Christie (1980). We apply this range of porosity-depth relationships to correct the reconstructed bathymetry for compaction of pre-MSC sediment at each step in our reconstruction.

Water loads for drawdown and reflooding phases have a density of standard seawater in our models (1,030 kg/$m^3$), although the real density during the evaporite deposition phases was likely higher due to the formation of more saline waters and brines (1,200 kg/$m^3$ at halite saturation). This has no significance for the pre-evaporite topographic reconstruction before brine formation at the Mediterranean scale, as the density increase cancels out with the later restoration of open marine conditions during the Zanclean flood.

An additional mechanism that modifies the depth of the Western Mediterranean basins is the cooling of the lithosphere. We use plate cooling models relating ocean floor depth to extensional age and heat flow (McKenzie, 1967; Parsons & Sclater, 1977; Stein & Stein, 1992) and continental extension models (McKenzie, 1978) to constrain this component of post-Messinian vertical motions. For the Provençal and Algerian Basins a MOR cooling model (Stein & Stein, 1992) is used, whereas for the Valencia Basin which consists of extended continental crust we use the McKenzie (1978) model. Dannowski et al. (2020) propose a failed rift and extended continental crust rather than full oceanic crust underlying the Ligurian Basin, which is the northeastern continuation of the Provençal Basin. However, as this region is not covered by our dataset and the Provençal Basin represents the wider and older part of this extensional domain we see no strong motivation to apply a continental crustal model to the Provençal Basin. The application of such a model would yield slightly smaller thermal subsidence values and deeper estimates of Messinian bathymetry in the basin.

# 4 | RESULTS

## 4.1 | Thermal subsidence

Fitting the limits of the opening ages of the Algerian (8–16 ma) and Provençal (16–22) basins to the oceanic plate model GDH1 (Stein & Stein, 1992) yields post-Messinian thermal subsidence of 250–325 m in the Provençal basin, and 325–435 m for the Algerian basin.

The Valencia Basin has been studied extensively regarding its crustal structure and extensional mechanisms (Maillard & Mauffret, 1999; Maillard et al., 1992; Negredo et al., 1999; Torné et al., 1992; Watts & Torné, 1992a, 1992b). Best-fit basin histories suggest a finite rifting model with an extension between 24 and 10 Ma, and the stretching factor ($\beta$) increasing from 1.4 on the basin flanks to three in the central basin (Watts & Torné, 1992a). Applying the McKenzie (1978) model yields a post-Messinian component of thermal subsidence in the range of 50–100 m on the flanks and 90–180 m in the centre depending on the applied post-rift age. Tectonic subsidence curves show a gradually decaying curve (Watts et al., 1990) meaning part of the thermal relaxation took place during the rifting phase and instantaneous rifting assumed in the McKenzie model does not apply to the Valencia Basin, so true values will fall towards the lower end of this range. Backstripping of wells in the Catalan margin area has yielded tectonic post-Messinian subsidence values ranging from 0 to 300 m (Bartrina et al., 1992; Watts & Torné, 1992a), with this variation in values possibly being related to ongoing activity on normal faults on the margin. Modelling of the basin evolution based on similar geodynamic data yielded maximum post-rift subsidence values of 380 m in the central part of the Valencia Basin since 10 Ma (Negredo et al., 1999). Due to the limitations of such 1D subsidence calculations we do not include the thermal component directly in our planform backstripping, as we are not able to constrain the lateral distribution of subsidence magnitudes accurately. However, we consider these subsidence values in the restored depths per basin presented in Table 2. Although thermal subsidence constitutes a considerable part of total vertical motions in the deep basins, because this effect diminishes towards the margins we consider that it introduces a minor (<100 m) uncertainty in the reconstructed depths of our shorelines.

## 4.2 | Effective elastic thickness

The results of our EET determination shown in Figure 5 yield an EET range of 10–45 km in the offshore domain

**TABLE 2** Bathymetry of Western Mediterranean sub-basins in modern day and at key moments during MSC, sediment thicknesses and vertical motion components

| Basin | | Liguro-Provençal | Algerian | Valencia | Halite CMD | Formentera | Cogedor |
|---|---|---|---|---|---|---|---|
| Average bathymetry | Modern | 2,700 | 2,820 | 1,500 | 950 | 1,680 | 620 |
| | UU level ( SL −1,100) | 2,300–2,755 | 2,120–2,610 | 1,110–1,420 | 775–920 | 1,302–1,442 | 206–311 |
| | UU level (no SL drop) | 2,650–3,105 | 2,470–2,970 | 1,460–1,770 | 980–1,125 | 1,618–1,767 | 455–560 |
| | BES level (SL −1,500) | 2,270–2,690 | 2,120–2,575 | 1,085–1,395 | 825–970 | 1,292–1,432 | 127–232 |
| | BES level (no SL drop) | 2,750–3,170 | 2,595–3,055 | 1,435–1,745 | 1,030–1,175 | 1,687–1,827 | 422–527 |
| | Pre-halite (drawdown) scenario | 3,020–3,325 | 2,915–3,255 | 1,485–1,795 | 1,280–1,425 | 1,832–1,972 | 543–648 |
| | Pre-halite (no drawdown) | 2,800–3,105 | 2,695–3,045 | 1,435–1,745 | 1,235–1,380 | 1,687–1,827 | 443–548 |
| Average sediment thickness | Plio-Quaternary | 1,325 | 818 | 920 | 295 | 220 | 190 |
| | Upper unit | 545 | 480 | 50 | 95 | 160 | 55 |
| | Mobile unit | 665 | 505 | — | 215 | 70 | 75 |
| | Total | 2,535 | 1,803 | 970 | 605 | 450 | 320 |
| Average subsidence of base MU | Plio-Quaternary | 640 | 390 | 500 | 60 | 75 | 150 |
| | Refilling | 350 | 350 | 300 | 205 | 325 | 250 |
| | Upper unit | 350 | 300 | 25 | 45 | 100 | 90 |
| | Rise sea-level | 130 | 125 | 50 | 0 | 70 | 45 |
| | Mobile unit | 340 | 235 | — | 10 | 70 | 100 |
| | Drawdown | −700 | −695 | −400 | −250 | −540 | −395 |
| | Compaction pre-MSC | 550–780 | 340–570 | 150–410 | 45–190 | 55–195 | 30–135 |
| | Thermal | 250–325 | 325–435 | 50–100 | 0 | 0 | 0 |
| | Total | 1,910–2,215 | 1,370–1,710 | 675–985 | 115–260 | 155–295 | 292–397 |

Average values are presented, but strong variations in sediment thicknesses and depths occur throughout the basins. In the CMD values correspond the average in the area of current halite occurrence. Paleodepth is determined by modern bathymetry - thickness sediment + decompaction pre-Messinian sediment + flexural-isostatic and thermal subsidence.

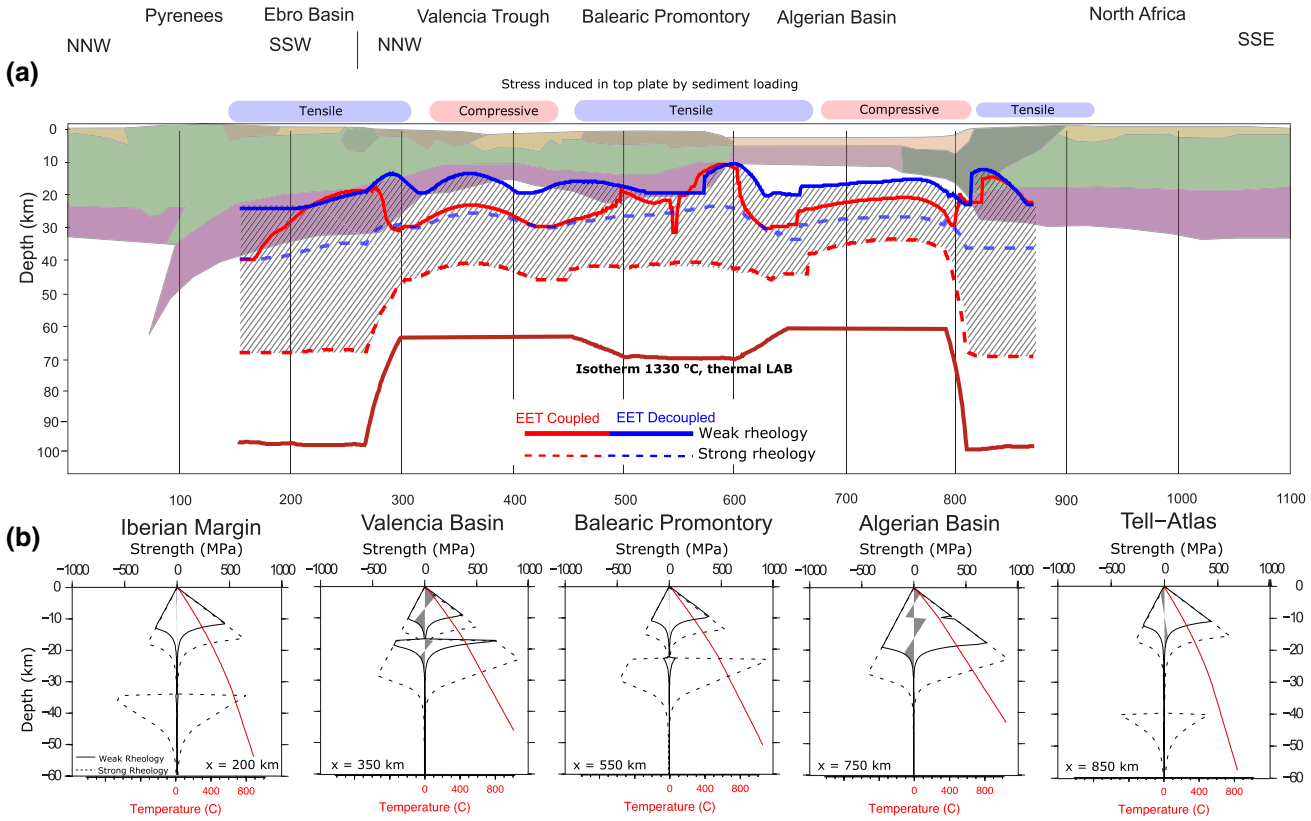


**FIGURE 5** (a) Effective elastic thickness (EET) variation from tAo model along a NE Iberia Geo-Transect (see Figure 1 for location). Crustal units with different density, heat production and thermal conductivity used for constructing geotherms derived from a compilation of crustal structural data (colour filled bodies) and thermal lithosphere-asthenosphere boundary (LAB, red-dark line) from Carballo et al. (2015). EET values determined for weak and strong rheological parameters for lower crust and upper mantle from Govers and Wortel (1995) and Cloetingh and Burov (1996) and for coupled versus decoupled crust and mantle. EET values are determined using tAo code by constructing Yield Strength Envelopes along transect based on rheology, geotherms and induced bending stresses by sediment loading since onset MSC. Range of plausible EET values hashed. Also shown is the stress regime induced on top of the plate by bending due to loading of sediment since onset MSC. (b) Yield Strength Envelopes constructed per region for weak and strong rheological parameters for lower crust and upper mantle from Govers and Wortel (1995) and Cloetingh and Burov (1996), showing decoupling in all regions but the Algerian Basin. Included are used geotherms and stresses (shaded grey area) at reference points along the section

with limited variation, with slightly lower values in the Algerian Basin. On the Emile Baudot Escarpment and the Algerian margin, we see sharp changes in EET values for weaker rheologies, likely due to bending stresses induced by boundaries of the sedimentary load in the deep basin.

European EET has been studied in this region by other authors using two principally different approaches. One is based on analysis of the spectral coherence of gravity anomalies and topography accounting for density variation in sediment, yielding values of 5–12 km in the Western Mediterranean basins (Kaban et al., 2018). Alternatively, EET is inferred by integrating the strength of the lithosphere derived from modelling based on thermal and rheological data, yielding values of <30 km for the Western Mediterranean (Tesauro et al., 2009).

The low strength estimated at the base of the crust along our 2D profile (from 0 MPa in the Iberian and north African margins to a maximum of 150 MPa in the Valencia Basin, see Figure 5) suggests a high degree of decoupling between crust and mantle in all regions except the Algerian Basin, which is the only region with true oceanic crust. This decoupling argues in support of using EETs towards the lower end value of our range, close to the 15 km value adopted for the 1D backstripping in Urgeles et al. (2011); and the Cenozoic evolution of the Catalan Coastal Ranges (5 km; Gaspar-Escribano et al., 2004). In addition, the generally low EET values (<20 km, Kaban et al., 2018) in the area derived from recent spectral analysis and the likelihood of decoupling between crust and lithospheric mantle in recently extended continental crust such as the Valencia Basin (Tesauro et al., 2009) point

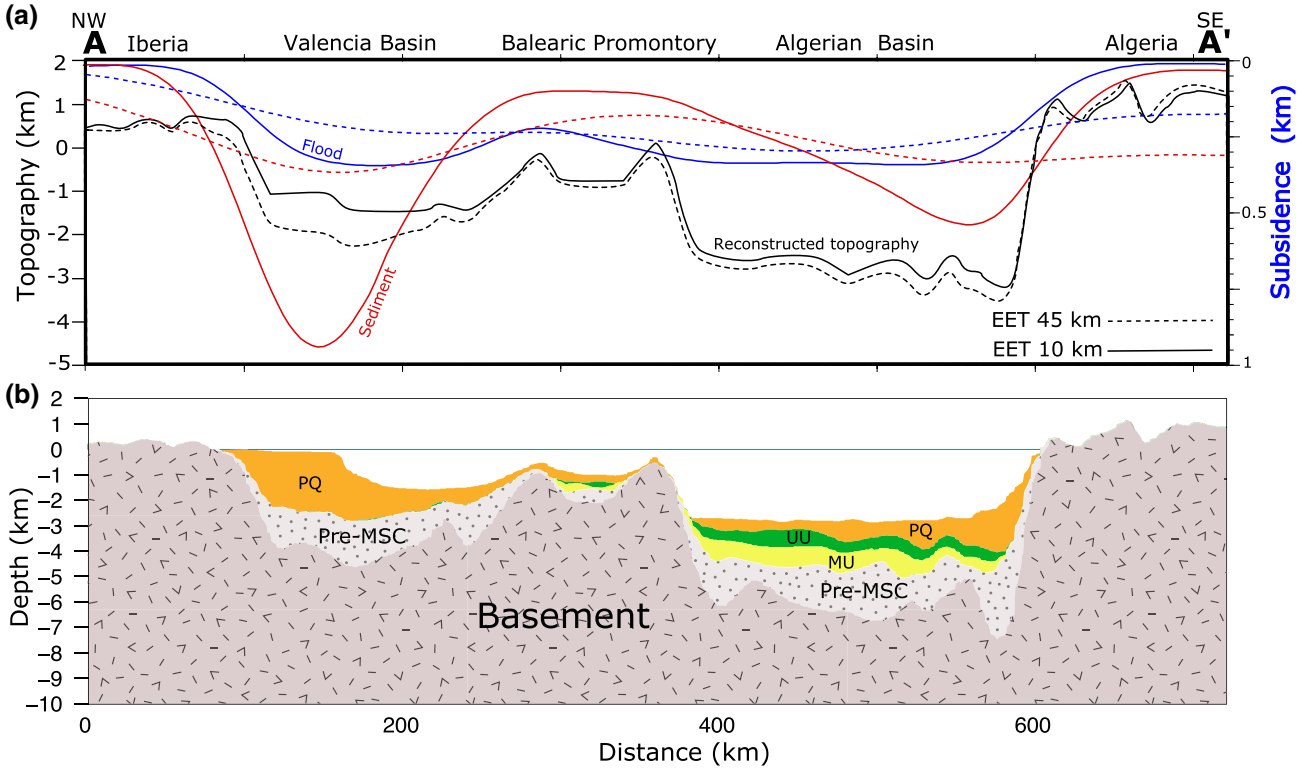


**FIGURE 6** (a) Schematic overview of results of backstripped profile A (see Figure 1 for location) for 10 and 45 km EET. Black: Reconstructed topography at end MSC, before deposition PQ sediment and water level at −1,000 m. Blue: vertical motions caused by 1 km change in water level (subsidence due to flooding). Orange: vertical motion due to sedimentation of Plio-Quaternary sediment (post-MSC subsidence). (b) Bathymetry and thicknesses of stratigraphic units used in backstripping along profile A. Orange: Plio-Quaternary sediment, green: in deep basin: upper unit, on Balearic Promontory: Bedded unit 3, Yellow: Mobile unit, Light Grey: Pre-MSC sediment, dark grey: basement

to values in the lower end of the range presented in Figure 5.

## 4.3 | Sensitivity of paleotopography to EET

In Figure 6 the sensitivity of our reconstructed topography after removing the PQ sediment and a 1 km water column to the end-member EET values is presented along cross section A (see Figure 1 for location). The reconstructed topography is strongly dependent on EET value in the Ebro delta region, where the Plio-Quaternary sediment load is largest. Here the localisation of flexural-isostatic subsidence leads to a >700 m difference in post-MSC subsidence, also affecting the slope of the reconstructed bottom shelf which is nearly flat in the 10 km EET scenario but has a significant basinward slope for a 45 km EET (Figure 6). In the steepest areas of the MES on the Iberian margin where the onlaps of UU are located the sensitivity of topography is still around 500 m, illustrating the importance of the EET parameter when constraining the magnitude of water level changes. Considering the arguments for relatively low EET values in the previous section we adopt an EET value of 15 km for our reference model and vary this parameter between 10 and 20 km to test the uncertainty of reconstructed paleoshoreline depths due to lithospheric strength. Reconstructed shoreline depths vary by ±100 m as a result of this variation.

## 4.4 | Sensitivity of paleoshoreline position to water level

The magnitude of a drop in water level during the MSC has a two-fold effect on the position of the reconstructed shoreline. First, it controls the magnitude of vertical motions affecting bathymetry, and secondly, it determines the depth of the isobath followed by the shoreline. Figure 7 presents the sensitivity of the model output shoreline position at different drawdown magnitudes for our reference 15 km EET value, both for the UU level and the BES level. The reconstructed shoreline positions presented in

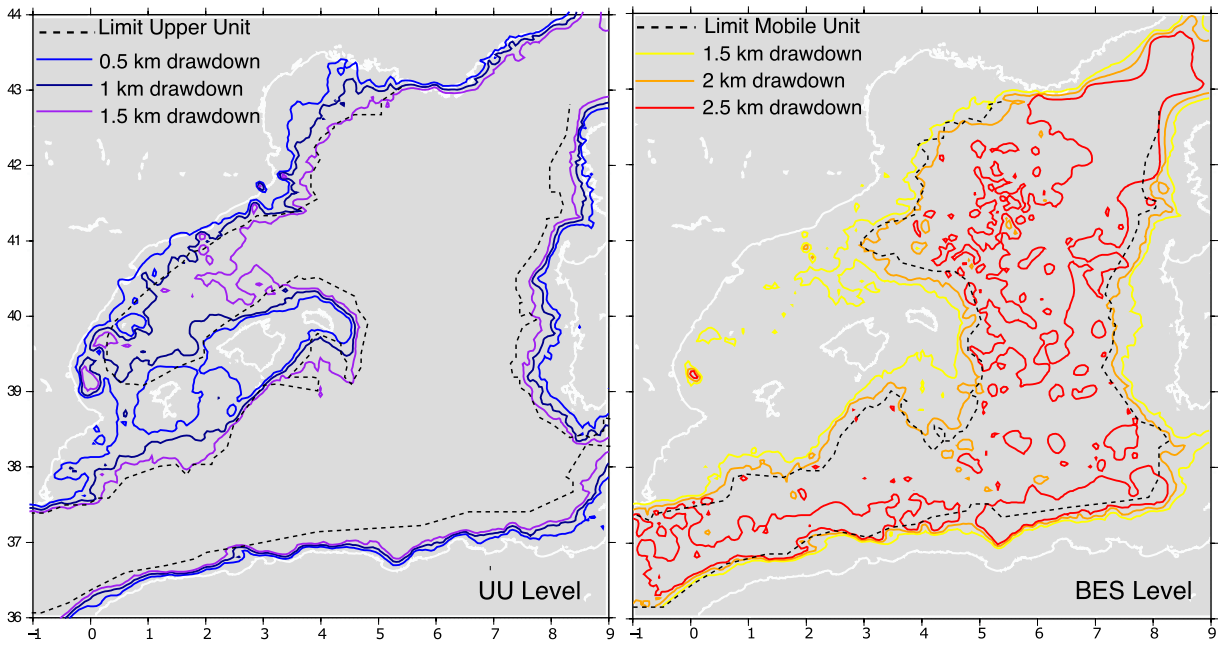


**FIGURE 7** Sensitivity of the calculated paleoshoreline to the magnitude of water level fall (EET = 15 km). Dashed black lines: position of paleoshoreline markers (see Figure 1). Solid lines: reconstructed isobaths for various water levels. Left: UU level, right: BES level

Figure 7 are not corrected for thermal subsidence or tectonic deformation since the MSC. This is done due to the lack of lateral constraints on these components discussed in Section 4.1.

In the Valencia Basin the most notable discrepancies in the paleoshoreline position for the UU level (Figure 10b) are located at the Columbretes volcano, which caused Pliocene-recent deformation of the MES and Valencia Fault, active from Miocene to Pliocene which offsets the MES by about 0.5 s TWTT (Maillard & Mauffret, 2013). Accounting for the max value of 325 m post-MSC thermal subsidence in the Provençal basin (see Section 4.1) would shift the reconstructed shorelines slightly basinward, as the margin of the basin was in reality shallower than in our reconstruction. In the Valencia Basin this adjustment is not necessary for our UU level reconstruction considering that post-MSC thermal subsidence on its margins was negligible. On the Algerian margin, the magnitude of the required adjustment is unclear, as subsidence in this area also carries a potential signal of tectonic origin due to subduction initiation and southward tilting of the basin (Auzende et al., 1972; Leprêtre et al., 2013; Yelles et al., 2009) affecting the depth of both the MU and UU limits. In the Valencia Basin, the UU limit in the Ebro delta region is likely not accurate, as Urgeles et al. (2011) showed the absence of a UU in their 3D dataset. Rather, they interpret the Messinian 'unit C' as a shallow water detrital fan. A water level of −1,300 m is required to expose the Ebro margin in this region. However, the water level cannot have been much lower as connectivity must have been maintained between the eastern Valencia Basin and the southwest Valencia Basin where the UU limit is clearly identified and mapped by Cameselle and Urgeles (2017) varying around a reconstructed depth of −1,100 m, although this connection is obscured by post-Messinian volcanic activity in the Columbretes. In the Gulf of Lions, the Upper unit limit lies considerably deeper, close to the reconstructed shoreline for a −1,500 m water level. In the steep Algerian Margin and Emile Baudot Escarpment, the UU limit lies further basinward than even the −2,000 m isobath. Tentatively, we suggest this might be related to the resedimentation of gypsum on steep margins, a process that does not require subaerial exposure (de Lange & Krijgsman, 2010) combined with tectonic processes mentioned above. As shoreline positions are better defined in the Valencia Basin where data availability is good and we can constrain our water level estimate against that of Urgeles et al. (2010) we consider this the more representative of paleo water level, rather than the deep basin margins where the depth of the UU limit is affected by the aforementioned processes. We, therefore, choose −1,100 ± 100 m as our reference water level for the UU level.

For the BES level, the limit of the MU fits well with a −1,500 m water level in the shallowest MU limit towards the Valencia Basin, which indicated the minimum water level drop required to expose the top of the halite in that region. The depth of the salt limit shows strong variations between −1,300 and −2,000 m within the Gulf of Lions,

whereas it is consistently deeper than −2,000 m along the margins of the deep basins.

The modern salt limit is affected by significant halokinetic activity (Badji et al., 2015; Dal Cin et al., 2016). This, combined with the basin scale tilting of the Algerian Basin mentioned above could explain the discrepancy between our reconstructed shorelines and the limit of both UU and MU in the deep basin margins, but the larger (approximately 2,200 m) drawdown required to obtain paleoshorelines in the position of the deep basin evaporite limit would imply a largely exposed sea floor in the Algerian basin (Figure 7), with only small local lakes. We choose −1,500 m for the BES level value as it allows for complete exposure of the BES in the Valencia Basin, but recognise that this constrains a minimum drop in water level which might still have been considerably lower at moments during the lowstand, as evidenced by the possible continuation of the BES underneath the MU.

### 4.5 | Reference model

Based on the results presented above, our reference model assumes a 15 km EET and water levels of −1,100 ± 100 m for UU level, which is the shallowest value for UU deposition found in places with a well-constrained UU limit, although it should be noted that the UU is absent in some areas with a deeper reconstructed bathymetry, that is the Ebro Margin.

The BES level in our reference model lies at −1,500 ± 100 m, which is the minimum water level drop needed to subaerially expose the BES to salt limit in the Valencia Basin, with the salt limit substantially deeper in other areas. In the Gulf of Lions our BES level shoreline along the ´Christiane' profile presented by Ryan (1976) is located at −2,050 ± 100 m, which fits well with their result of −1,900 depth for the Late Messinian, even though we do not account for the isostatic effects of erosion in this region.

In the no-drawdown scenario, our potential shorelines are positioned approximately 200 m deeper than when the flexural effect of removal of the water column is considered.

Each panel in Figure 8 represents a single step in our reconstruction and can be interpreted as the flexural-isostatic effect on the Base MU surface of the applied load. The drop in water level at step 5 (Figure 8e) results in a large rebound of up to 700 m in the deep basins, causing basin-wide shallowing even significantly affecting the margins and Balearic Promontory. The change in water level between BES and UU levels (Figure 8d) and UU deposition (Figure 8c) are not able to undo the entirety of this rebound, and the basins remain at their shallowest point throughout these steps. This strongly affects the bathymetry and depth of paleoshoreline markers formed during the BES and UU levels. The reflooding (Figure 8b) and subsequent sedimentation (Figure 8a) restore the basins to close to their pre-drawdown depth. The flexural-isostatic subsidence by sediment loading (Figure 9a) was accompanied by compaction of the pre-halite sediment underlying the MSC units (Figure 9b), and the total vertical motion on the Base MU surface since the onset of MU deposition is presented in Figure 9c.

The final resulting topography and shoreline positions, accounting for compaction and flexural-isostatic motions are presented in Figure 10. These maps exclude the thermal subsidence, in which lateral variations are not accurately constrained. This explains the differences in reconstructed depths between Figure 10 and Table 2, where Table 2 represents the more accurate reconstructed depths. For the BES and UU levels, the topography including (Figure 10c,e) and excluding (Figure 10d,f) water level drop is presented.

## 5 | DISCUSSION

A key outstanding question around the MSC concerns the spatial distribution of evaporites and its link to paleo water depths. We describe the evolution of the Western Mediterranean basins from the perspective of our flexural-isostatic reconstruction for each sub-basin starting from the pre-Messinian bathymetry, and the implications for the paleoenvironmental changes during the MSC.

Assuming the paleoshoreline-based constraints on water level during the MSC are correct, our flexural-isostatic reconstruction shows that bathymetry of the intermediate basins before the onset of halite deposition (Figure 10b) was slightly deeper than today, having since undergone subsidence by compaction, isostatic compensation and thermal cooling that combined was smaller than the sediment fill. The Valencia Basin reached 1,500–1,800 m depending on the chosen compaction curve (Table 2, Figure 10b), and underwent a maximum of 1,100 m of subsidence since the MSC (Figure 9c). Because the UU in the Valencia Basin is relatively thin and MU is absent, its depth in our reconstruction during the MSC is controlled primarily by water level and the PQ load. The pre-halite depths of the Algerian and Provençal basins reached about 3 km depth on average (Figure 10b, Table 2), which is similar to the present-day bathymetry. They underwent between 1,200 and 2,000 m of subsidence since the MSC (Figure 9c) which is close to the sediment thickness accumulated in that same period. The significantly greater depth of the Provençal and Algerian basins compared to the intermediate basins can explain the much larger salt thickness, as they were not

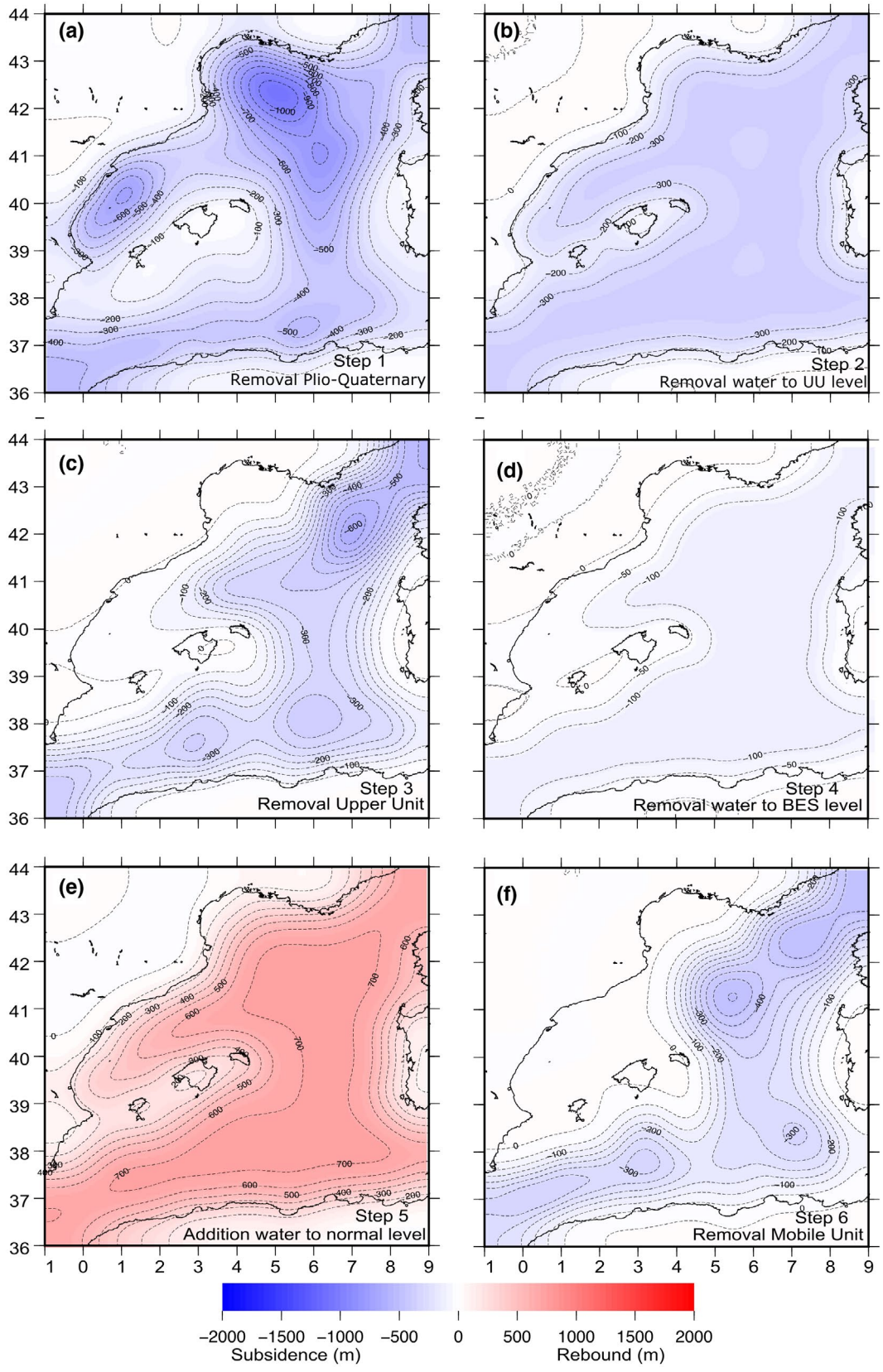


**FIGURE 8** Flexural-isostatic vertical motions in m corresponding to each step of our reference model scenario. Sedimentation and floodings caused subsidence represented by negative values (blue), whereas water level drop caused rebound represented by positive values (red). Not included are the effects of onshore erosion/sedimentation

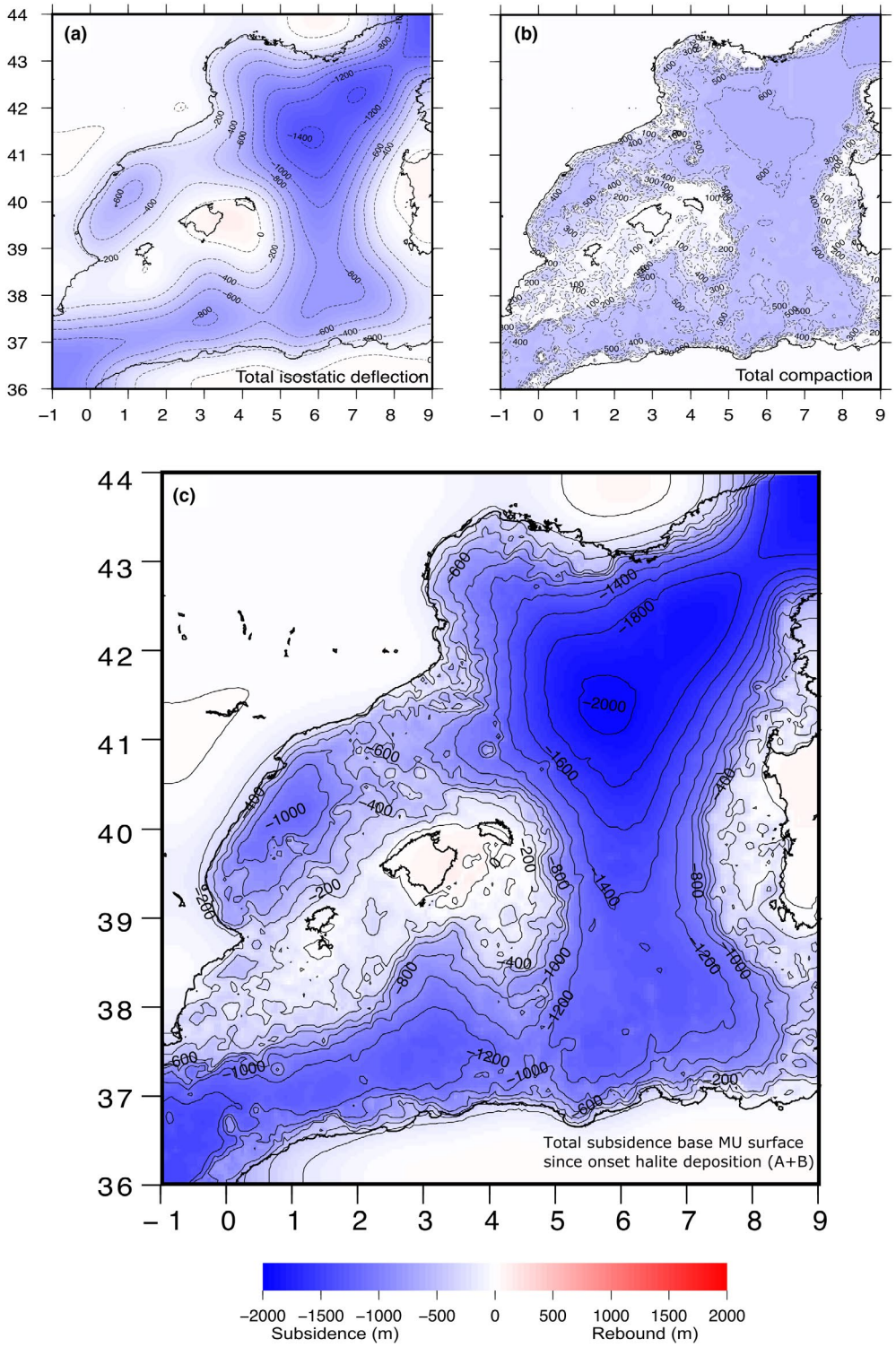


**FIGURE 9** (a) Sum of flexural-isostatic vertical motions in m since the onset of halite deposition, for the reference setup. (b) Total compaction of pre-halite sediment. (c) Total subsidence of the base of Messinian sediment and MES since the onset of MU deposition (A + B). All values for reference model scenario. Not included are effects of onshore erosion/sedimentation and thermal subsidence

as extensively exposed during the drawdown stage. In addition, any exposed and dissolved salt would be trapped, in contrast to the Valencia Basin, from which it could be transported to the deep basins.

The water column above the top halite surface at the end of the MU deposition in the deep basins was approximately 2,700–3,300 m if halite was deposited in high water (Manzi et al., 2005), and 700–1,200 m if the drawdown to

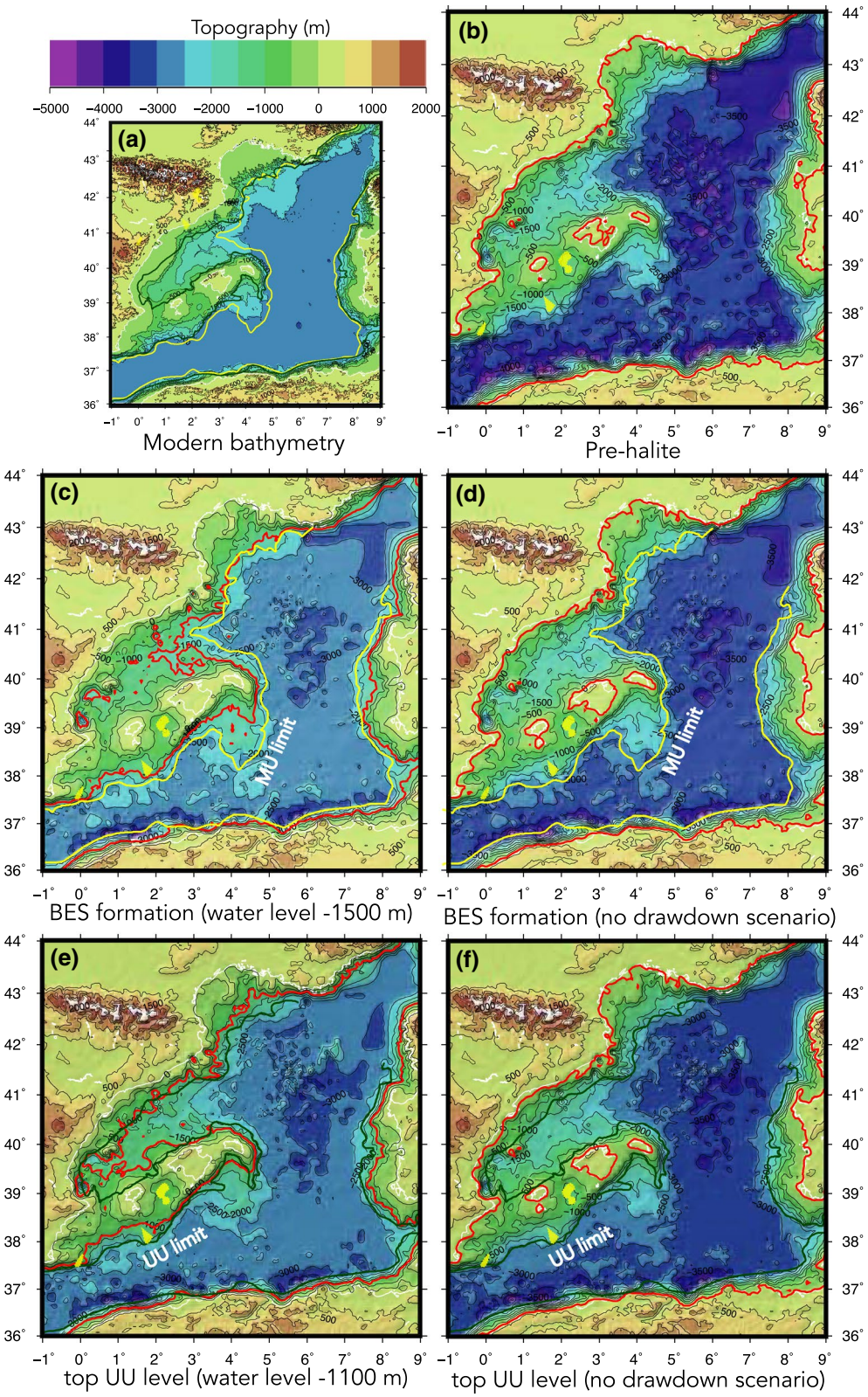


**FIGURE 10** Modern topography (a) and reconstructed paleobathymetry results for our reference setup. These maps are not compensated for the thermal subsidence effect, overestimating the depth of the deep basins. (b) Pre-halite deposition. (c) BES level (top MU) with water level at −1,500. (d) Alternative BES level (top MU) for no-drawdown scenario. (e) UU level (top UU) with water level at −1,100. (f) Alternative UU level (top UU) with for no-drawdown scenario. Yellow line in (c, d): limit MU, green line in (e, f): limit UU. Solid red line: reconstructed shoreline. Yellow: halite isolated halite patches in CMD, Formentera and Cogedor basins. Note the discrepancy in required water level at the BES and UU levels of approximately 400 m in the drawdown scenarios (c vs. e)

BES level (of 1,500 m) occurred. At the halite limit in the Valencia Basin, this water column pre-drawdown was still 2 km, reducing to 0 after the drawdown.

In our reference model the uplift induced by the water level drop (Figure 8e), yields basins shallower than today during the UU deposition. If our best-fit water level of −1,100 m at the UU level is correct (in accordance with proposed values by Cameselle et al., 2014, Maillard et al., 2006, slightly higher than previous estimates by Urgeles et al., 2011; Mas et al., 2018) this implies a maximum water depth of approximately 400 m at the transition from the Valencia Basin to the deep basin (Figure 10e) at the end of UU deposition, and shallower (300–350 m) if we correct for thermal subsidence. At the same time, water depth in the deep basins reached 1,000–1,600 (average) to 2,000 (max) m (Figure 10e), which might suggest a different sedimentary environment and consequently a change in the nature of the UU between the Provençal Basin and the Valencia Basin. Without this drawdown isostatic effect, the topography of the basins is 300 m deeper in the basin centres and water depths are therefore up to 3,400 m (Figure 10f).

In the no-drawdown scenario (Figure 10d,f) we see that halite preservation occurs from laterally variable depths, from 1,500 m (western Gulf of Lions) to 2,500 m in the Valencia Basin and 3,000–3,500 m in the deep basins (Figure 10d). These discrepancies could be explained by halokinetic activity, but the absence of halite in the Valencia Basin cannot be explained by such a mechanism alone, so either precipitation in that region must be prevented by a so-far unidentified mechanism, or halite must have been removed by submarine dissolution/erosion up to a very considerable depth (at least 2,500 m) which we consider unlikely. The onlap depth of the UU in this scenario is also very variable, from 500 to 1,000 m in the Valencia Basin to 2,500 m in the deep basins, and considerable thickness of the UU is only reached at depths >2,500 m. Considering the clastic nature of the UU, it is hard to explain these trends in a high water level scenario considering that the Valencia Basin and shallower margins would have had the biggest sediment supply. We therefore do not favour this scenario.

The main sources of uncertainty are the poor constraints on the EET and compaction of pre-halite sediment, as well as the magnitude of erosion in the exposed parts of the basin during the drawdown. We observe a disconnection between the UU and Bedded unit 3 lying on the Balearic Promontory (map in Figure 11), onlapping on both sides of a topographic high situated between the CMD and Valencia Basin. Assuming this sill was exposed and considering the depth of this high when compensating for post-Messinian sedimentation, this indicates that the water level was at some point at least 600–750 m below modern sea level. Moreover, the onlaps of Bedded unit 3 in the CMD are positioned at a reconstructed depth of 750–900 m at the UU level, which is shallower than those of the UU on the southwest margin of the Valencia Basin (>1,000 m). This supports the interpretation that stage 3 MSC deposits in the CMD (Bedded unit 3) were accumulated in isolated basins perched above the Valencia Basin water level. It implies deposition in an independent hydrological environment from the deep basin controlled by erosion and resedimentation on the Balearic Promontory.

On the Balearic Promontory, the halite patches (Figures 1 and 11) occur at a wide range of present-day depths. Halite precipitation in the CMD depocenter started at a depth of 1,280–1,425 m, depending on the decompaction curve applied for the pre-halite sediment (see Table 2). Halite also deposited in basins with a restored depth as shallow as 550–660 m (Cogedor) which pre-halite depth could be as shallow as 450 m if we assume no drawdown ever occurred, as this close to the margin the remnant uplift of the −1,500 m change in water level in our reference model affects the pre-halite bathymetry. However, here we do not account for post-Messinian tectonics. Constraining these in this area is difficult due to the complex way the Balearic Promontory deformed, with large variations along its structure. Its western part (near Alicante shelf) was deformed by compression (Maillard & Mauffret, 2013) the vertical component of which would not have been more than 200–300 m. The true paleodepth might thus have been deeper, up to 960 m but the magnitude of this effect is not well constrained. The aforementioned effect of residual shallowing due to the −1,500 m drawdown also affects the Formentera Basin, which has a reconstructed depth of 1,830–1,970 m pre-halite but could be 150 m shallower if no drawdown occurred.

A striking feature in these patches is the absence of any halite thickness versus paleodepth relationship (Figure 11d). The deepest pre-MSC basin (Figure 11c, Formentera) has a much thinner halite unit than the CMD (Figure 11a), which was lying up to 500 m shallower at the onset of the MU deposition (see Table 2 for depths and thicknesses). This could suggest that halite thickness in these patches was controlled by the local geometry of the basins and possibly the depths of their outlets. The open nature of the Cogedor and Formentera basins (Figure 10), with respect to the completely silled-off CMD, might have made them more susceptible to dissolution of the halite during the lowstand. Dissolved salt in Cogedor and Formentera would escape to the deep basin, whereas in the CMD it is trapped inside the depression. This has been hypothesised by Raad et al. (2021) for the CMD, and a similar scenario has been proposed for the outcropping Sicilian halite (García-Veigas et al., 2018). It should be

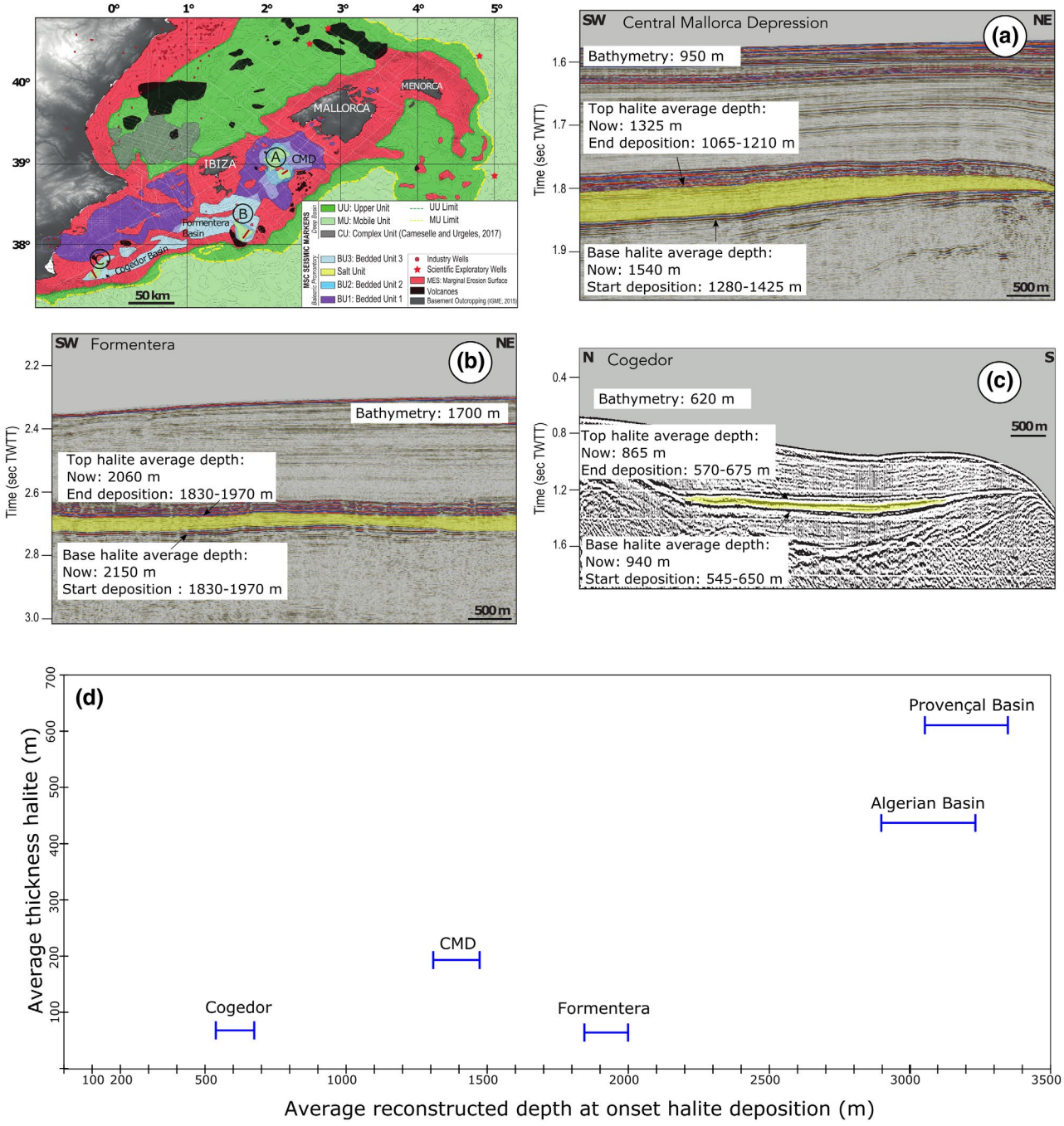


**FIGURE 11** Seismic images of halite patches in CMD (a), Cogedor (b) and Formentera (c) basins showing current top and base depth of the halite (yellow) in TWTT (ms). Included are the reconstructed paleo-depths of both horizons not including the effect of water unloading. Map from Raad et al. (2021). (d) Relationship of halite thickness to average reconstructed depth. Although the maximum thickness is reached in the deep basins, the smaller halite patches show no thickness-depth relationship

noted that especially on the western Balearic Promontory and potentially in the CMD, the effect of tectonic deformation since the MSC should be accounted for in order to achieve a higher accuracy in the paleodepth restoration. This is beyond the scope of this paper but will shed more light on the role of the sills related to the halite patches during their formation.

Halite is conspicuously absent in the Valencia Basin, which had a pre-halite depth reaching at least 1,500 m (Table 2). This can tentatively be explained as follows: it has been proposed by several authors that halite deposition occurred in deep water, in a strongly stratified water column (Simon & Meijer, 2017; Yoshimura et al., 2016). Any brine formed in the Valencia Basin may have sunk towards

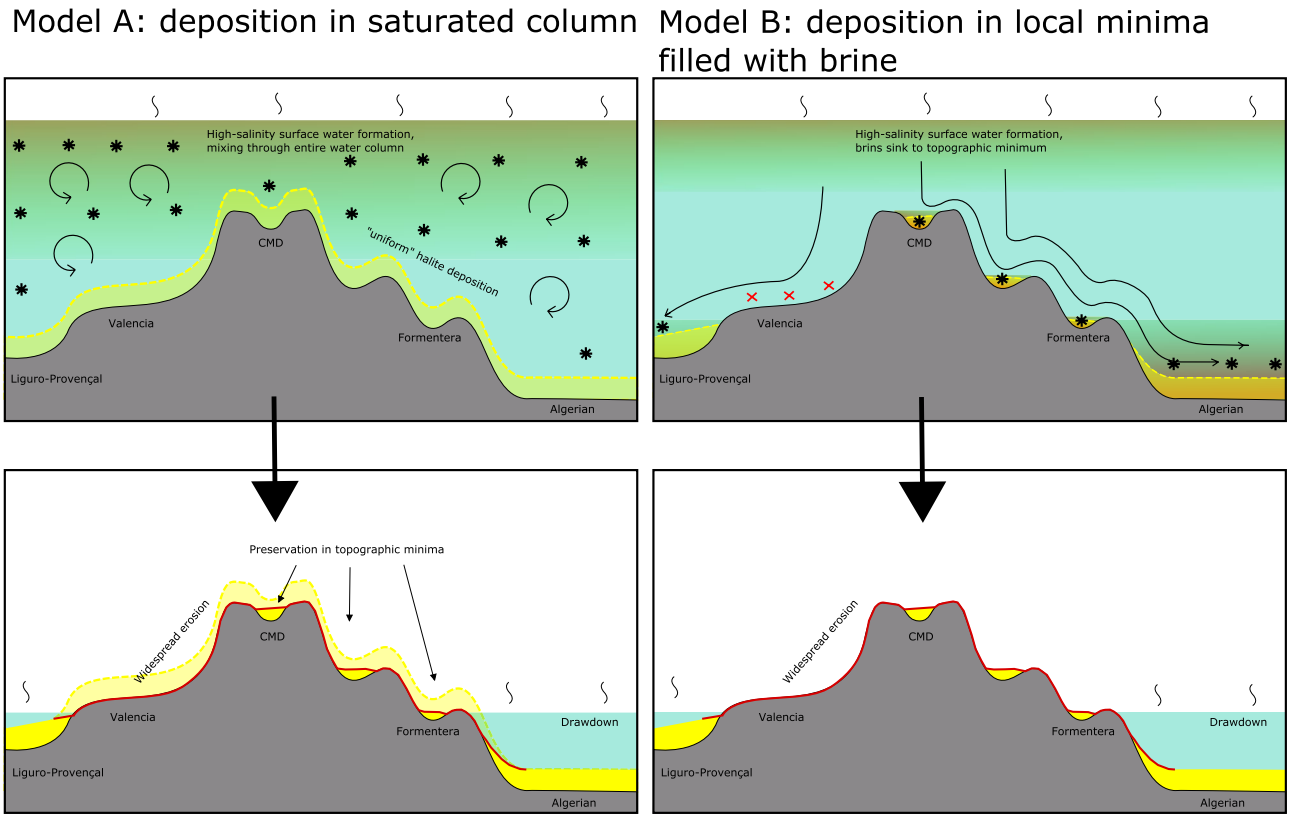


**FIGURE 12** Contrasting models of halite deposition explaining the current depth-thickness distribution of halite. (a) Halite is deposited throughout/in the top of the water column over the entire region, and subsequent drawdown exposes the intermediate basins removing all halite. In topographic minima, some halite is preserved, as well as in the seep basins. (b) Halite is deposited in local minima where dense brine can accumulate, whereas the Valencia Basin which is deeper than the CMD does not see halite accumulation because the dense brine sinks towards the deep basin. In this scenario, the thickness of deposited halite in local minima depends on the geometry of the depressions

the deep Provençal Basin, as there was no topographic sill in between, although we could reasonably expect some salt trapping in the westernmost part of the Valencia Basin where volcanic edifices and structural highs were already present and depth variations allowed for the deposition of the MSC-related Complex Unit related to the lowstand (Cameselle & Urgeles, 2017). Alternatively, halite was deposited on the floor of the Valencia Basin but was later dissolved/eroded during the BES lowstand (−1,500 m) when the basin floor was subaerially exposed. A combination of both processes is not excluded. These contrasting models are presented in Figure 12. Our results do not allow us to distinguish between these models, but the reconstructed depths of the basins do evidence the importance of explaining the observed halite distribution.

The flexural-isostatic effect of the deep-basin isostatic loads on Mallorca Island suggests a close to zero effect (Figure 9c) of vertical motion by MSC events, as rebound due to the drawdown (Figure 8e) was reversed by flooding and Plio-Quaternary sedimentation (Figure 8a,b). Based on the volume of post-Messinian sediment lying on the Balearic Promontory platform offshore (see Appendix B), we estimate the isostatic erosional rebound assuming it was eroded from the current onshore Balearic Islands (effect not included in Figures 8–10 due to their relative magnitudes). Using the constraints outlined in Section 3.2, the eroded mass onshore is equivalent to a uniform load of 130–310 m. It should be noted that this height does not account for porosity changes from consolidated rock to sediment, so their true height would be smaller, but the mass removed from the islands is not affected by this simplification. We also do not account for the onshore post-MSC sedimentation in the Palma graben (see Capó & Garcia, 2019 for thickness maps onshore), which suggest that the central part of Mallorca island was not exposed to erosion until recently. This implies the rebound due to erosion would be more concentrated on the NW and SE regions of the island than shown in our results (see Appendix B). The erosion magnitude yields an average erosion rate of 0.03–0.04 mm/year over the Pliocene and Quaternary, which is on the same order of magnitude as measured rates of seacliff erosion (Balaguer & Fornós, 2003). The rebound on the Balearic Islands due to erosion affects the pre-Messinian reefs on the eastern coast

of Mallorca by up to 60 m since the MSC. We tentatively suggest that this explains the present-day elevation of the terminal carbonate complex on Mallorca island, originally formed near sea level (Mas & Fornós, 2013) and that a higher eustatic sea-level before the MSC is not required to explain the elevation of phreatic overgrowths on speleothems as proposed by Dumitru et al. (2021). Previous estimates of long-term deformation on the eastern shore of Mallorca based on six Pliocene sea-level indicators yielded a median value of 0.002 mm/year (Dumitru et al., 2019), which would yield a total post-MSC uplift of approximately 10 m, which is significantly below our estimate.

Another important outcome of our results on the Balearic Promontory and the margins of the deep basins is the potentially large differential rebound and subsidence resulting from sudden drawdown and refilling events (see Figure 8b,d,e). Although the subsidence and rebound induced by sedimentation and erosion develop gradually, the water level changes associated with the MSC are thought to have happened over very short time lapses (a few thousand years for the drawdown; Garcia-Castellanos & Villaseñor, 2011; Meijer & Krijgsman, 2005; and a few years for the reflooding; Garcia-Castellanos et al., 2009), implying geologically-instantaneous changes in the surface isostatic loading. Thus, the isostatic time response is limited by the viscosity of the asthenosphere and forced to be also very rapid (stress relaxation in the asthenosphere takes place in time periods of about 20 kyr; Watts, 2001; Watts et al., 2013). Since the density contrast between water, air and asthenosphere lead to a 0.3–0.4 ratio of the flexural response relative to the water level change, the kilometric drawdown imposed vertical motions in excess of several hundred metres in the aforementioned time scales. Because the uplift due to water level drop was reversed during subsequent stages, lasting effects on the deep basins are hard to distinguish in the modern basin, although it has been linked to a basin-wide magmatic pulse (Sternai et al., 2017). On the margins, these events caused differential motions of up to 700 m over a distance of about 100 km (Figure 8), which could result in (re)activation of fault systems. Evidence for a tectonic response to this rebound would be very distinct from general normal fault activity, as it could be expressed as a phase of tectonic inversion. Although so far such evidence has not been described, it could independently strengthen the water level fall hypothesis for the MSC.

Our water level estimate implies a disconnection between the western and eastern Mediterranean at the platform between Sicily and Tunisia throughout a large part of MSC stage 3. The current depth of the Sicily Sill is 430 m, although its paleodepth during the crisis is not well constrained (Blanc, 2006). A recent study shows that the isostatic subsidence caused on the Malta platform due to sediment accumulation in the Ionian Sea during the PQ is very minor (Micallef et al., 2018). Assuming the sill was there during the MSC, this means that water levels in the Eastern and Western basins were decoupled and dependent on local hydrological budgets and that during the reflooding of the basin water level would have remained stagnant at the level of the Sicily Sill until water levels in the Eastern Basin reached that of the sill, as previously suggested by (Blanc, 2006; Garcia-Castellanos & Villaseñor, 2011; Lofi et al., 2005; Meijer & Krijgsman, 2005) and supported by terrace formation at various depths in different parts of the Mediterranean (Just et al., 2011; Micallef et al., 2018 and references therein).

## 6 | CONCLUSIONS

We present a reconstruction of Messinian paleotopography in the Western Mediterranean accounting for the flexural-isostatic response to sedimentation and water level variations since the onset of the Messinian Salinity Crisis. We test a scenario in which the main drawdown phase follows the emplacement of the MU (salt), and where the overlying UU is emplaced in shallow waters, contrasted with a model without drawdown. Combining a thermo-mechanically constrained flexural-isostatic modelling, we arrive at the following conclusions:

1. If the BES surface was formed by subaerial erosional processes, then the level of the Western Mediterranean water surface was at least as low as $-1{,}500 \pm 100$ m prior to UU deposition.
2. If the extent of the UU deposits mark the coeval paleoshoreline, then the water level was no higher than $-1{,}100 \pm 100$ m at the end of the UU deposition.
3. The 1,500-m-drawdown scenario would imply a 700-m rebound of the deep basins causing the basins to be significantly shallower during the final stage of the MSC compared to times preceding and following the MSC lowstand.
4. The isostatic subsidence, compaction and thermal subsidence since the Messinian largely compensate the accumulation of sediment, implying that the bathymetry of the various basins at the onset of MU deposition was similar to the modern day.
5. There exists no thickness-paleodepth relationship for halite in the perched CMD, Formentera and Cogedor basins. We interpret this lack of a trend, together with the absence of halite in the deeper Valencia Basin, as the result of halite being deposited or preserved only in local bathymetric minima, with the halite thickness being controlled by the depth of such depressions and their outlets (e.g. spillways of brine to deeper regions).

## ACKNOWLEDGMENTS

We thank the reviewers, Bill Ryan and Valentin Rime, for their constructive and comprehensive comments that greatly improved the manuscript. All members of the SALTGIANT community are thanked for the inspirational discussions during workshops, courses and fieldtrips. Funding was provided by the European Commission through ITN *SaltGiant* (Horizon2020-765256) and partly by GeoCAM (PGC2018-095154-B-100), Spanish Government. This work was done using the facilities of the Laboratory of Geodynamic Modelling at Geo3BCN-CSIC. Figures were produced using the free software Generic Mapping Tools (Wessel et al., 2013). We acknowledge the 'Archivo Técnico de Hidrocarburos of the Spanish Ministerio de Industria Comercio' for having provided the SPBAL seismic data used in this study. The study also includes seismic profiles obtained from the SIGEOF database of the Instituto Geologico y Minero de España (IGME, www.igme.es). We acknowledge Schlumberger Company for providing the academic license of the seismic interpretation software Petrel. D. Garcia-Castellanos designed and supervised the study. H. Heida was primarily responsible for the modelling and writing of the manuscript. F. Raad interpreted seismic data and described the Messinian seismic record. D. Garcia-Castellanos and I. Jiménez-Munt oversaw the TISC and lithosphere modelling procedure. A. Maillard and J. Lofi contributed seismic data and interpretation of Mediterranean geology. All authors contributed to and made edits to the manuscript.

## CONFLICT OF INTEREST

The authors certify that they have no affiliations with or involvement in any organisation or entity with any financial or non-financial interest (such as personal or professional relationships, affiliations, knowledge or beliefs) in the subject matter or materials discussed in this manuscript.

## PEER REVIEW

The peer review history for this article is available at https://publons.com/publon/10.1111/bre.12610.

## DATA AVAILABILITY STATEMENT

Input and output grids, as well as scripts used for the modelling, are available at GitHub: https://github.com/hanneke heida/TISC_WestMediterranean.git. TISC is available as free software from: https://github.com/danigeos/tisc.

## ORCID

*Hanneke Heida* https://orcid.org/0000-0001-5456-896X
*Fadl Raad* https://orcid.org/0000-0002-7143-2420

## REFERENCES

Acosta, J., Ancochea, E., Canals, M., Huertas, M. J., & Uchupi, E. (2004). Early Pleistocene volcanism in the Emile Baudot Seamount, Balearic Promontory (western Mediterranean Sea). *Marine Geology*, *207*, 247–257. https://doi.org/10.1016/j.margeo.2004.04.003

Acosta, J., Muñoz, A., Herranz, P., Palomo, C., Ballesteros, M., Vaquero, M., & Uchupi, E. (2001). Geodynamics of the Emile Baudot Escarpment and the Balearic Promontory, western Mediterranean. *Marine and Petroleum Geology*, *18*, 349–369, 00003-4. https://doi.org/10.1016/S0264-8172(01)00003-4

Alvarez, W. (1972). Rotation of the Corsica-Sardinia microplate. *Nature Physical Sciences*, *235*, 103–105. https://doi.org/10.1038/physci235103a0

Amadori, C., Garcia-Castellanos, D., Toscani, G., Sternai, P., Fantoni, R., Ghielmi, M., & Di Giulio, A. (2018). Restored topography of the Po Plain-Northern Adriatic region during the Messinian base-level drop-Implications for the physiography and compartmentalization of the palaeo-Mediterranean basin. *Basin Research*. https://doi.org/10.1111/bre.12302

Andreetto, F., Aloisi, G., Raad, F., Heida, H., Flecker, R., Agiadi, K., Lofi, J., Blondel, S., Bulian, F., Camerlenghi, A., Caruso, A., Ebner, R., Garcia-Castellanos, D., Gaullier, V., Guibourdenche, L., Gvirtzman, Z., Hoyle, T. M., Meijer, P. T., Moneron, J., … Krijgsman, W. (2021). Freshening of the Mediterranean Salt Giant: Controversies and certainties around the terminal (Upper Gypsum and Lago-Mare) phases of the Messinian Salinity Crisis. *Earth Science Reviews*, *216*, 103577. https://doi.org/10.1016/j.earscirev.2021.103577

Andreetto, F., Matsubara, K., Beets, C. J., Fortuin, A. R., Flecker, R., & Krijgsman, W. (2020). High Mediterranean water-level during the Lago-Mare phase of the Messinian Salinity Crisis: Insights from the Sr isotope records of Spanish marginal basins (SE Spain). *Palaeogeography, Palaeoclimatology, Palaeoecology*, *562*, 110139. https://doi.org/10.1016/j.palaeo.2020.110139

Auzende, J. M., Olivet, J. L., & Bonnin, J. (1972). Une structure compressive au nord de l'Algérie? *Deep Sea Research and Oceanographic Abstracts*, *19*, 149–155. https://doi.org/10.1016/0011-7471(72)90047-2

Bache, F., Olivet, J. L., Gorini, C., Rabineau, M., Baztan, J., Aslanian, D., & Suc, J. P. (2009). Messinian erosional and salinity crises: View from the Provence Basin (Gulf of Lions, Western Mediterranean). *Earth and Planetary Science Letters*, *286*, 139–157. https://doi.org/10.1016/j.epsl.2009.06.021

Badji, R., Charvis, P., Bracene, R., Galve, A., Badsi, M., Ribodetti, A., Benaissa, Z., Klingelhoefer, F., Medaouri, M., & Beslier, M.-O. (2015). Geophysical evidence for a transform margin offshore Western Algeria: A witness of a subduction-transform edge propagator? *Geophysical Journal International*, *200*, 1029–1045. https://doi.org/10.1093/gji/ggu454

Balaguer, P., & Fornós, J. J. (2003). Erosive processes at Eastern Mallorca seacliffs (Illes Balears, western Mediterranean): Evaluation of erosion rates by granular disgregation, Preliminary data. *Bolletí de la Societat d'Història Natural de les Balears*, *46*.

Bartrina, M. T., Cabrera, L., Jurado, M. J., Guimerà, J., & Roca, E. (1992). Evolution of the central Catalan margin of the Valencia trough (western Mediterranean). *Tectonophysics*, *203*, 219–247. https://doi.org/10.1016/0040-1951(92)90225-U

Bellucci, M., Pellen, R., Leroux, E., Bache, F., Garcia, M., Do Couto, D., Raad, F., Blondel, S., Rabineau, M., Gorini, C., Moulin, M., Maillard, A., Lofi, J., Del Ben, A., Camerlenghi, A., Poort, J. & Aslanian, D. (2021). A comprehensive and updated compilation of the seismic stratigraphy markers in the Western Mediterranean Sea. SEANOE. https://doi.org/10.17882/80128

Bessis, F. (1986). Some remarks on the study of subsidence of sedimentary basins Application to the Gulf of Lions margin (Western Mediterranean). *Marine and Petroleum Geology*, *3*, 37–63. https://doi.org/10.1016/0264-8172(86)90055-3

Blanc, P. L. (2002). The opening of the plio-quaternary gibraltar strait: Assessing the size of a cataclysm. *Geodinamica Acta*, *15*, 303–317. https://doi.org/10.1080/09853111.2002.10510763

Blanc, P. L. (2006). Improved modelling of the Messinian Salinity Crisis and conceptual implications. *Palaeogeography, Palaeoclimatology, Palaeoecology*, *238*, 349–372. https://doi.org/10.1016/j.palaeo.2006.03.033

Bourillot, R., Vennin, E., Rouchy, J. M., Blanc-Valleron, M. M., Caruso, A., & Durlet, C. (2010). The end of the Messinian Salinity Crisis in the western Mediterranean: Insights from the carbonate platforms of south-eastern Spain. *Sedimentary Geology*, *229*, 224–253. https://doi.org/10.1016/j.sedgeo.2010.06.010

Bourillot, R., Vennin, E., Rouchy, J. M., Durlet, C., Rommevaux, V., Kolodka, C., & Knap, F. (2009). Structure and evolution of a Messinian mixed carbonate-siliciclastic platform: The role of evaporites (Sorbas Basin, South-east Spain). *Sedimentology*, *57*, 477–512. https://doi.org/10.1111/j.1365-3091.2009.01092.x

Bulian, F., Sierro, F. J., Ledesma, S., Jiménez-Espejo, F. J., & Bassetti, M.-A. (2021). Messinian West Alboran Sea record in the proximity of Gibraltar: Early signs of Atlantic-Mediterranean gateway restriction. *Marine Geology*, *434*, 106430. https://doi.org/10.1016/j.margeo.2021.106430

Burov, E. B., & Diament, M. (1995). The effective elastic thickness (Te) of continental lithosphere: What does it really mean? *Journal of Geophysical Research*, *100*, 3905–3927. https://doi.org/10.1029/94JB02770

Burrus, J. (1984). Contribution to a geodynamic synthesis of the Provençal Basin (North-Western Mediterranean). *Marine Geology*, *55*, 247–269. https://doi.org/10.1016/0025-3227(84)90071-9

Camerlenghi, A., Accettella, D., Costa, S., Lastras, G., Acosta, J., Canals, M., & Wardell, N. (2009). Morphogenesis of the SW Balearic continental slope and adjacent abyssal plain, Western Mediterranean Sea. *International Journal of Earth Sciences*, *98*, 735–750. https://doi.org/10.1007/s00531-008-0354-8

Cameselle, A. L., & Urgeles, R. (2017). Large-scale margin collapse during Messinian early sea-level drawdown: The SW Valencia trough, NW Mediterranean. *Basin Research*, *29*, 576–595. https://doi.org/10.1111/bre.12170

Cameselle, A. L., Urgeles, R., De Mol, B., Camerlenghi, A., & Canning, J. C. (2014). Late Miocene sedimentary architecture of the Ebro Continental Margin (Western Mediterranean): Implications to the Messinian Salinity Crisis. *International Journal of Earth Sciences*, *103*, 423–440. https://doi.org/10.1007/s00531-013-0966-5

Capó, A., & Garcia, C. (2019). Basin filling evolution of the central basins of Mallorca since the Pliocene. *Basin Research*, *31*, 948–966. https://doi.org/10.1111/bre.12352

Carballo, A., Fernandez, M., Torne, M., Jiménez-Munt, I., & Villaseñor, A. (2015). Thermal and petrophysical characterization of the lithospheric mantle along the northeastern Iberia geo-transect. *Gondwana Research*, *27*, 1430–1445. https://doi.org/10.1016/j.gr.2013.12.012

CIESM. (2008). The Messinian Salinity Crisis from mega-deposits to microbiology – A consensus report. CIESM Workshop Monographs, CIESM Workshop Monographs.

Clauzon, G., Suc, J. P., Couto, D. D., Jouannic, G., Melinte-Dobrinescu, M. C., Jolivet, L., Quillévéré, F., Lebret, N., Mocochain, L., Popescu, S. M., Martinell, J., Doménech, R., Rubino, J. L., Gumiaux, C., Warny, S., Bellas, S. M., Gorini, C., Bache, F., Rabineau, M., & Estrada, F. (2015). New insights on the Sorbas Basin (SE Spain): The onshore reference of the Messinian Salinity Crisis. *Marine and Petroleum Geology*, *66*, 71–100. https://doi.org/10.1016/j.marpetgeo.2015.02.016

Clauzon, G., Suc, J. P., Gautier, F., Berger, A., & Loutre, M. F. (1996). Alternate interpretation of the Messinian salinity crisis: Controversy resolved? *Geology*, *24*, 363–366. https://doi.org/10.1130/0091-7613(1996)024<0363:AIOTMS>2.3.CO;2

Cloetingh, S., & Burov, E. B. (1996). Thermomechanical structure of European continental lithosphere: Constraints from rheological profiles and EET estimates. *Geophysical Journal International*, *124*, 695–723. https://doi.org/10.1111/j.1365-246X.1996.tb05633.x

Comas, M. C., Zahn, R., Klaus, A., Mascle, J., Lohmann, G. P., & Clift, P. D. (1996). Proceedings of the ocean drilling program, initial reports. *Ocean Drilling Program*, *158*, 114–177. https://doi.org/10.2973/odp.proc.ir.161.105.1996

Conesa, G., & Badinot, J. F. (1999). Early Messinian carbonate platforms from Sorbas Basin (SE Spain): Sedimentary setting, microfaunas and palaeoenvironments. *Revue De Micropaléontologie*, *42*, 255–267.

Cornée, J. J., Saint Martin, J. P., Conesa, G., Münch, P., André, J. P., Saint Martin, S., & Roger, S. (2004). Correlations and sequence stratigraphic model for Messinian carbonate platforms of the western and central Mediterranean. *International Journal of Earth Sciences*, *93*, 621–633. https://doi.org/10.1007/s00531-004-0400-0

Dabrio, C. J., & Polo Camacho, M. D. (1995). Oscilaciones eustáticas de alta frecuencia en el Neógeno superior de Sorbas (Almería, sureste de España). *GeoActa*, *18*, 75–78.

Dal Cin, M., Del Ben, A., Mocnik, A., Accaino, F., Geletti, R., Wardell, N., Zgur, F., & Camerlenghi, A. (2016). Seismic imaging of Late Miocene (Messinian) evaporites from Western Mediterranean back-arc basins. *Petroleum Geoscience*, *22*, 297–308. https://doi.org/10.1144/petgeo2015-096

Dannowski, A., Kopp, H., Grevemeyer, I., Lange, D., Thorwart, M., Bialas, J., & Wollatz-Vogt, M. (2020). Seismic evidence for failed rifting in the Ligurian Basin, Western Alpine domain. *Solid Earth*, *11*, 873–887. https://doi.org/10.5194/se-11-873-2020

de Lange, G. J., & Krijgsman, W. (2010). Messinian salinity crisis: A novel unifying shallow gypsum/deep dolomite formation mechanism. *Marine Geology*, *275*, 273–277. https://doi.org/10.1016/j.margeo.2010.05.003

Decima, A., & Wezel, F. C. (1967). Late Miocene Evaporites of the Central Sicilian Basin, Italy. Deep Sea Drilling Project Initial Reports (Vol. *13*).

Dela Pierre, F., Bernardi, E., Cavagna, S., Clari, P., Gennari, R., Irace, A., Lozar, F., Lugli, S., Manzi, V., Natalicchio, M., Roveri, M., & Violanti, D. (2011). The record of the Messinian salinity crisis in the Tertiary Piedmont Basin (NW Italy): The Alba section

revisited. *Palaeogeography, Palaeoclimatology, Palaeoecology*, *310*, 238–255. https://doi.org/10.1016/j.palaeo.2011.07.017

Do Couto, D., Gumiaux, C., Jolivet, L., Augier, R., Lebret, N., Folcher, N., Jouannic, G., Suc, J. P., & Gorini, C. (2015). 3D modelling of the Sorbas Basin (Spain): New constraints on the Messinian Erosional Surface morphology. *Marine and Petroleum Geology*, *66*, 101–116. https://doi.org/10.1016/j.marpetgeo.2014.12.011

Driussi, O., Maillard, A., Ochoa, D., Lofi, J., Chanier, F., Gaullier, V., Briais, A., Sage, F., Sierro, F., & Garcia, M. (2015). Messinian Salinity Crisis deposits widespread over the Balearic Promontory: Insights from new high-resolution seismic data. *Marine and Petroleum Geology*, *66*, 41–54. https://doi.org/10.1016/j.marpetgeo.2014.09.008

Dronkert, H. (1976). Late miocene evaporites in the Sorbas Basin and adjoining areas. *Bollettino della Società Geologica Italiana*, *16*, 341–361.

Dronkert, H. (1985). Evaporite models and sedimentology of Messinian and Recent Evaporites. GUA papers of geology. Series 1.

Dumitru, O. A., Austermann, J., Polyak, V. J., Fornós, J. J., Asmerom, Y., Ginés, J., Ginés, A., & Onac, B. P. (2019). Constraints on global mean sea level during Pliocene warmth. *Nature*, *574*, 233–236. https://doi.org/10.1038/s41586-019-1543-2

Dumitru, O. A., Austermann, J., Polyak, V. J., Fornós, J. J., Asmerom, Y., Ginés, J., Ginés, A., & Onac, B. P. (2021). Sea-level stands from the Western Mediterranean over the past 6.5 million years. *Scientific Reports*, *11*(1), 1–10. https://doi.org/10.1038/s41598-020-80025-6

Escutia, C., & Maldonado, A. (1992). Palaeogeographic implications of the Messinian surface in the Valencia trough, northwestern Mediterranean Sea. *Tectonophysics*, *203*, 263–284. https://doi.org/10.1016/0040-1951(92)90227-W

Estrada, F., Ercilla, G., Gorini, C., Alonso, B., Vázquez, J. T., García-Castellanos, D., Juan, C., Maldonado, A., Ammar, A., & Elabbassi, M. (2011). Impact of pulsed Atlantic water inflow into the Alboran Basin at the time of the Zanclean flooding. *Geo-Marine Letters*, *31*, 361–376. https://doi.org/10.1007/s00367-011-0249-8

Etheve, N., Mohn, G., Frizon de Lamotte, D., Roca, E., Tugend, J., & Gómez-Romeu, J. (2018). Extreme Mesozoic crustal thinning in the eastern Iberia margin: The example of the Columbrets Basin (Valencia Trough). *Tectonics*, *37*, 636–662. https://doi.org/10.1002/2017TC004613

Faccenna, C., Piromallo, C., Crespo-Blanc, A., Jolivet, L., & Rossetti, F. (2004). Lateral slab deformation and the origin of the western Mediterranean arcs. *Tectonics*, *23*, 1–21. https://doi.org/10.1029/2002TC001488

Fortuin, A. R., Krijgsman, W., Hilgen, F. J., & Sierro, F. J. (2000). Late Miocene Mediterranean desiccation: Topography and significance of the 'Salinity Crisis' erosion surface on-land in southeast Spain: Comment. *Sedimentary Geology*, *133*, 167–174. https://doi.org/10.1016/S0037-0738(00)00040-3

Galdeano, A., & Rossignol, J. C. (1977). Contribution de l'aeromagnetisme a l'etude du golfe de Valence (Mediterranee occidentale). *Earth and Planetary Science Letters*, *34*, 85–99. https://doi.org/10.1016/0012-821X(77)90109-1

Gallart, J., Vidal, N., Estévez, A., Pous, J., Sàbat, F., Santisteban, C., & Surinach, E.; Group, E.V.T. (1995). The ESCI-València Troug Vertical reflection Experiment: A Seismic Image of the Crust from the NE Iberian Peninsula to the Western Mediterranean. *Revista De La Sociedad Geologica De Espana*, *8*(4), 401–415.

Garcia-Castellanos, D., Estrada, F., Jiménez-Munt, I., Gorini, C., Fernàndez, M., Vergés, J., & De Vicente, R. (2009). Catastrophic flood of the Mediterranean after the Messinian salinity crisis. *Nature*, *462*, 778–782. https://doi.org/10.1038/nature08555

Garcia-Castellanos, D., Fernàndez, M., & Torne, M. (1997). Numerical modeling of foreland basin formation: A program relating thrusting, flexure, sediment geometry and lithospehre rheology. *Computers & Geosciences*, *23*, 993–1003. https://doi.org/10.1016/S0098-3004(97)00057-5

Garcia-Castellanos, D., Fernández, M., & Torne, M. (2002). Modeling the evolution of the Guadalquivir foreland basin (southern Spain). *Tectonics*, *21*(3), 9-1–9-17. https://doi.org/10.1029/2001TC001339

Garcia-Castellanos, D., Micallef, A., Estrada, F., Camerlenghi, A., Ercilla, G., Periáñez, R., & Abril, J. M. (2020). The Zanclean megaflood of the Mediterranean – Searching for independent evidence. *Earth Science Reviews*, *201*, 103061. https://doi.org/10.1016/j.earscirev.2019.103061

Garcia-Castellanos, D., & Villaseñor, A. (2011). Messinian salinity crisis regulated by competing tectonics and erosion at the Gibraltar arc. *Nature*, *480*, 359–363. https://doi.org/10.1038/nature10651

García-Veigas, J., Cendón, D. I., Gibert, L., Lowenstein, T. K., & Artiaga, D. (2018). Geochemical indicators in Western Mediterranean Messinian evaporites: Implications for the salinity crisis. *Marine Geology*, *403*, 197–214. https://doi.org/10.1016/j.margeo.2018.06.005

Gargani, J. (2004). Modelling of the erosion in the Rhone valley during the Messinian crisis (France). *Quaternary International*, *121*, 13–22. https://doi.org/10.1016/j.quaint.2004.01.020

Gaspar-Escribano, J. M., Garcia-Castellanos, D., Roca, E., & Cloetingh, S. (2004). Cenozoic vertical motions of the Catalan Coastal Ranges (NE Spain): The role of tectonics, isostasy, and surface transport: Vertical motions CCR (NE Spain). *Tectonics*, *23*, 1–18. https://doi.org/10.1029/2003TC001511

Gaullier, V., Loncke, L., Vendeville, B. C., Deverchere, J., Droz, L., Obone Zue Obane, E. M. & Mascle, J. (2008). Salt tectonics in the deep Mediterranean: Indirect clues for understanding the Messinian Salinity Crisis. In *The Messian Salinity Crisis from mega-deposits to microbiology – A consensus report*.

Gelabert, B., Sàbat, F., & Rodríguez-Perea, A. (2002). A new proposal for the late Cenozoic geodynamic evolution of the western Mediterranean. *Terra Nova*, *14*, 93–100. https://doi.org/10.1046/j.1365-3121.2002.00392.x

Govers, R. (2009). Choking the Mediterranean to dehydration: The Messinian salinity crisis. *Geology*, *37*, 167–170. https://doi.org/10.1130/G25141A.1

Govers, R., Meijer, P., & Krijgsman, W. (2009). Regional isostatic response to Messinian Salinity Crisis events. *Tectonophysics*, *463*, 109–129. https://doi.org/10.1016/j.tecto.2008.09.026

Govers, R., & Wortel, M. J. R. (1995). Extension of stable continental lithosphere and the initiation of lithospheric scale faults. *Tectonics*, *14*, 1041–1055. https://doi.org/10.1029/95TC00500

Gueguen, E., Doglioni, C., & Fernandez, M. (1998). On the post-25 Ma geodynamic evolution of the western Mediterranean. *Tectonophysics*, *298*, 259–269. https://doi.org/10.1016/S0040-1951(98)00189-9

Haq, B., Gorini, C., Baur, J., Moneron, J., & Rubino, J. L. (2020). Deep Mediterranean's Messinian evaporite giant: How much salt? *Global and Planetary Change*, *184*, 103052. https://doi.org/10.1016/j.gloplacha.2019.103052

Hsü, K. J., Ryan, W. B. F., & Cita, M. B. (1973). Late Miocene dessication of the Mediterranean. *Nature*, *242*, 240–244.

Jolivet, L., Augier, R., Robin, C., Suc, J. P., & Rouchy, J. M. (2006). Lithospheric-scale geodynamic context of the Messinian salinity crisis. *Sedimentary Geology*, *188–189*, 9–33. https://doi.org/10.1016/j.sedgeo.2006.02.004

Just, J., Hübscher, C., Betzler, C., Lüdmann, T., & Reicherter, K. (2011). Erosion of continental margins in the Western Mediterranean due to sea-level stagnancy during the Messinian Salinity Crisis. *Geo-Marine Letters*, *31*, 51–64. https://doi.org/10.1007/s00367-010-0213-z

Kaban, M. K., Chen, B., Tesauro, M., Petrunin, A. G., El Khrepy, S., & Al-Arifi, N. (2018). Reconsidering effective elastic thickness estimates by incorporating the effect of sediments: A case study for Europe. *Geophysical Research Letters*, *45*, 9523–9532. https://doi.org/10.1029/2018GL079732

Krijgsman, W., Fortuin, A. R., Hilgen, F. J., & Sierro, F. J. (2001). Astrochronology for the Messinian Sorbas basin (SE Spain) and orbital (precessional) forcing for evaporite cyclicity. *Sedimentary Geology*, *140*, 43–60. https://doi.org/10.1016/S0037-0738(00)00171-8

Krijgsman, W., Hilgen, F. J., Raffi, I., Sierro, F. J., & Wilson, D. S. (1999). Chronology, causes and progession of the Messinian salinity crisis. *Nature*, *400*, 652–655.

Leprêtre, A., Klingelhoefer, F., Graindorge, D., Schnurle, P., Beslier, M. O., Yelles, K., Déverchère, J., & Bracene, R. (2013). Multiphased tectonic evolution of the Central Algerian margin from combined wide-angle and reflection seismic data off Tipaza, Algeria. *Journal of Geophysical Research: Solid Earth*, *118*, 3899–3916. https://doi.org/10.1002/jgrb.50318

Leroux, E., Aslanian, D., & Rabineau, M. (2019). *Atlas of the stratigraphic markers in the Western Mediterranean with focus on the Messinian, Pliocene and Pleistocene of the Gulf of Lion*. Commission de la carte géologique du monde.

Lofi, J. (2018). *Messinian Salinity Crisis markers in the Mediterranean Sea – Volume 2*. CGMW and Mémoires de la Société Géologie de France.

Lofi, J., Déverchère, J., Gaullier, V., Gillet, H., Gorini, C., Guennoc, P., Loncke, L., Maillard, A., Sage, F., & Thinon, I.; World, C. for the G.M. of the. (2011). *Seismic Atlas of the Messinian Salinity Crisis markers in the Mediterranean and Black Seas* (Vol. *179*). Memoires de la Société Géologique de France.

Lofi, J., Gorini, C., Berné, S., Clauzon, G., Dos Reis, A. T., Ryan, W. B. F., & Steckler, M. S. (2005). Erosional processes and paleoenvironmental changes in the Western Gulf of Lions (SW France) during the Messinian Salinity Crisis. *Marine Geology*, *217*, 1–30. https://doi.org/10.1016/j.margeo.2005.02.014

Lofi, J., Sage, F., Deverchere, J., Loncke, L., Maillard, A., Gaullier, V., Thinon, I., Gillet, H., Guennoc, P., & Gorini, C. (2011). Refining our knowledge of the Messinian salinity crisis records in the offshore domain through multi-site seismic analysis. *Bulletin De La Societe Geologique De France*, *182*, 163–180. https://doi.org/10.2113/gssgfbull.182.2.163

Lonergan, L., & White, N. (1997). Origin of the Betic-Rif mountain belt. *Tectonics*, *16*, 504–522. https://doi.org/10.1029/96TC03937

Lugli, S., Manzi, V., Roveri, M., & Schreiber, C. B. (2010). The Primary Lower Gypsum in the Mediterranean: A new facies interpretation for the first stage of the Messinian salinity crisis. *Palaeogeography, Palaeoclimatology, Palaeoecology*, *297*, 83–99. https://doi.org/10.1016/j.palaeo.2010.07.017

Lugli, S., Schreiber, B. C., & Triberti, B. (1999). Giant polygons in the Realmonte Mine (Agrigento, Sicily); Evidence for the desiccation of a Messinian halite basin. *Journal of Sedimentary Research*, *69*, 764–771. https://doi.org/10.2110/jsr.69.764

Maillard, A., Driussi, O., Lofi, J., Briais, A., Chanier, F., Hübscher, C., & Gaullier, V. (2014). Record of the Messinian Salinity Crisis in the SW Mallorca area (Balearic Promontory, Spain). *Marine Geology*, *357*, 304–320. https://doi.org/10.1016/j.margeo.2014.10.001

Maillard, A., Gaullier, V., Lézin, C., Chanier, F., Odonne, F., & Lofi, J. (2020). New onshore/offshore evidence of the Messinian Erosion Surface from key areas: The Ibiza-Balearic Promontory and the Orosei-Eastern Sardinian margin. *BSGF - Earth Sciences Bulletin*, *191*, 9. https://doi.org/10.1051/bsgf/2020007

Maillard, A., Gorini, C., Mauffret, A., Sage, F., Lofi, J., & Gaullier, V. (2006). Offshore evidence of polyphase erosion in the Valencia Basin (Northwestern Mediterranean): Scenario for the Messinian Salinity Crisis. *Sedimentary Geology*, *188–189*, 69–91. https://doi.org/10.1016/j.sedgeo.2006.02.006

Maillard, A., Jolivet, L., Lofi, J., Thinon, I., Couëffé, R., Canva, A., & Dofal, A. (2020). Transfer zones and associated volcanic province in the eastern Valencia Basin: Evidence for a hot rifted margin? *Marine and Petroleum Geology*, *119*, 104419. https://doi.org/10.1016/j.marpetgeo.2020.104419

Maillard, A., & Mauffret, A. (1993). Structure et volcanisme de la fosse de Valence (M{é}diterran{é}e nord-occidentale). *Bulletin De La Société Géologique De France*, *164*, 365–383.

Maillard, A., & Mauffret, A. (1999). Crustal structure and riftogenesis of the Valencia Trough (north-western Mediterranean Sea). *Basin Research*, *11*, 357–379. https://doi.org/10.1046/j.1365-2117.1999.00105.x

Maillard, A., & Mauffret, A. (2013). Structure and present-day compression in the offshore area between alicante and ibiza island (eastern iberian margin). *Tectonophysics*, *591*, 116–130. https://doi.org/10.1016/j.tecto.2011.07.007

Maillard, A., Mauffret, A., Watts, A. B., Torné, M., Pascal, G., Buhl, P., & Pinet, B. (1992). Tertiary sedimentary history and structure of the Valencia trough (western Mediterranean). *Tectonophysics*, *203*, 57–75. https://doi.org/10.1016/0040-1951(92)90215-R

Malinverno, A., & Ryan, W. B. F. (1986). Extension in the Tyrrhenian Sea and shortening in the Apennines as result of arc migration driven by sinking of the lithosphere. *Tectonics*, *5*, 227–245. https://doi.org/10.1029/TC005i002p00227

Manzi, V., Gennari, R., Hilgen, F., Krijgsman, W., Lugli, S., Roveri, M., & Sierro, F. J. (2013). Age refinement of the Messinian salinity crisis onset in the Mediterranean. *Terra Nova*, *25*, 315–322. https://doi.org/10.1111/ter.12038

Manzi, V., Gennari, R., Lugli, S., Persico, D., Reghizzi, M., Roveri, M., Schreiber, B. C., Calvo, R., Gavrieli, I., & Gvirtzman, Z. (2018). The onset of the Messinian salinity crisis in the deep Eastern Mediterranean basin. *Terra Nova*, *30*, 189–198. https://doi.org/10.1111/ter.12325

Manzi, V., Lugli, S., Lucchi, F. R., & Roveri, M. (2005). Deep-water clastic evaporites deposition in the Messinian Adriatic foredeep (northern Apennines, Italy): Did the Mediterranean

ever dry out? *Sedimentology*, *52*, 875–902. https://doi.org/10.1111/j.1365-3091.2005.00722.x

Manzi, V., Lugli, S., Roveri, M., & Charlotte Schreiber, B. (2009). A new facies model for the Upper Gypsum of Sicily (Italy): Chronological and palaeoenvironmental constraints for the Messinian salinity crisis in the Mediterranean. *Sedimentology*, *56*, 1937–1960. https://doi.org/10.1111/j.1365-3091.2009.01063.x

Manzi, V., Roveri, M., Gennari, R., Bertini, A., Biffi, U., Giunta, S., Iaccarino, S. M., Lanci, L., Lugli, S., Negri, A., Riva, A., Rossi, M. E., & Taviani, M. (2007). The deep-water counterpart of the Messinian Lower Evaporites in the Apennine foredeep: The Fanantello section (Northern Apennines, Italy). *Palaeogeography, Palaeoclimatology, Palaeoecology*, *251*, 470–499. https://doi.org/10.1016/j.palaeo.2007.04.012

Martí, J., Mitjavila, J., Roca, E., & Aparicio, A. (1992). Cenozoic Magmatism of the Valencia trough (western Mediterranean): Relationships between structural evolution and volcanism. *Tectonophysics*, *203*, 145–165.

Martínez-Martínez, J. M., & Azañón, J. M. (1997). Mode of extensional tectonics in the southeastern Betics (SE Spain): Implications for the tectonic evolution of the peri-Alborán orogenic system. *Tectonics*, *16*, 205–225. https://doi.org/10.1029/97TC00157

Mas, G., & Fornós, J. J. (2011). The Messinian Salinity Crisis Record in the Palma Basin (Mallorca, Balearic Islands, Western Mediterranean).

Mas, G., & Fornós, J. J. (2013). Late Messinian Lago-Mare deposits of the island of Mallorca (Western Mediterranean). Implications on the MSC events.

Mas, G., Maillard, A., Alcover, J. A., Fornós, J. J., Bover, P., & Torres-Roig, E. (2018). Terrestrial colonization of the Balearic Islands: New evidence for the Mediterranean sea-level drawdown during the Messinian Salinity Crisis. *Geology*, *46*, 527–530. https://doi.org/10.1130/G40260.1

Mauffret, A., Frizon de Lamotte, D., Lallemant, S., Gorini, C., & Maillard, A. (2004). E-W opening of the Algerian Basin (Western Mediterranean). *Terra Nova*, *16*, 257–264. https://doi.org/10.1111/j.1365-3121.2004.00559.x

Mauffret, A., Pascal, G., Maillard, A., & Gorini, C. (1995). Tectonics and deep structure of the north-western Mediterranean Basin. *Marine and Petroleum Geology*, *12*, 645–666. https://doi.org/10.1016/0264-8172(95)98090-R

McKenzie, D. P. (1967). Some remarks on heat flow and gravity anomalies. *Journal of Geophysical Research*, *72*, 6261–6273. https://doi.org/10.1029/jz072i024p06261

McKenzie, D. (1978). Some remarks on the development of sedimentary basins. *Earth and Planetary Science Letters*, *40*, 25–32. https://doi.org/10.1016/0012-821X(78)90071-7

Meijer, P., & Krijgsman, W. (2005). A quantitative analysis of the desiccation and re-filling of the Mediterranean during the Messinian Salinity Crisis. *Earth and Planetary Science Letters*, *240*, 510–520. https://doi.org/10.1016/j.epsl.2005.09.029

Meilijson, A., Hilgen, F., Sepúlveda, J., Steinberg, J., Fairbank, V., Flecker, R., Waldmann, N. D., Spaulding, S. A., Bialik, O. M., Boudinot, F. G., Illner, P., & Makovsky, Y. (2019). Chronology with a pinch of salt: Integrated stratigraphy of Messinian evaporites in the deep Eastern Mediterranean reveals long-lasting halite deposition during Atlantic connectivity. *Earth Science Reviews*, *194*, 374–398. https://doi.org/10.1016/j.earscirev.2019.05.011

Micallef, A., Camerlenghi, A., Garcia-Castellanos, D., Cunarro Otero, D., Gutscher, M. A., Barreca, G., Spatola, D., Facchin, L., Geletti, R., Krastel, S., Gross, F., & Urlaub, M. (2018). Evidence of the Zanclean megaflood in the eastern Mediterranean Basin. *Scientific Reports*, *8*, 1–8. https://doi.org/10.1038/s41598-018-19446-3

Negredo, A., Fernàndez, M., Torné, M., & Doglioni, C. (1999). Numerical modeling of simultaneous extension and compression: The Valencia trough (western Mediterranean). *Tectonics*, *18*, 361–374. https://doi.org/10.1029/1998TC900026

Norman, S. E., & Chase, C. G. (1986). Uplift of the shores of the western Mediterranean due to Messinian desiccation and flexural isostasy. *Nature*, *322*, 450–451. https://doi.org/10.1038/322450a0

Ochoa, D., Sierro, F. J., Lofi, J., Maillard, A., Flores, J. A., & Suárez, M. (2015). Synchronous onset of the Messinian evaporite precipitation: First Mediterranean offshore evidence. *Earth and Planetary Science Letters*, *427*, 112–124. https://doi.org/10.1016/j.epsl.2015.06.059

Orszag-Sperber, F. (2006). Changing perspectives in the concept of "Lago-Mare" in Mediterranean Late Miocene evolution. *Sedimentary Geology*, *188–189*, 259–277. https://doi.org/10.1016/j.sedgeo.2006.03.008

Ott d'Estevou, P., & Montenat, C. (1990). Le bassin de Sorbas-Tabernas. In *Les Bassins Neogenes Du Domaine Betique Oriental (Espagne)* (pp. 101–128).

Pagnier, H. (1976). Depth of deposition of Messinian selenitic gypsum in the Basin of Sorbas (SE Spain). *Bollettino della Società Geologica Italiana*, *16*, 363–367.

Parsons, B., & Sclater, J. G. (1977). An analysis of the variation of ocean floor bathymetry and heat flow with age. *Journal of Geophysical Research*, *82*, 803–827. https://doi.org/10.1029/jb082i005p00803

Pellen, R., Aslanian, D., Rabineau, M., Suc, J. P., Gorini, C., Leroux, E., Blanpied, C., Silenziario, C., Popescu, S. M., & Rubino, J. L. (2019). The Messinian Ebro River incision. *Global and Planetary Change*, *181*, 102988. https://doi.org/10.1016/j.gloplacha.2019.102988

Raad, F., Lofi, J., Maillard, A., Tzevahirtzian, A., & Caruso, A. (2021). The Messinian Salinity Crisis deposits in the Balearic Promontory: An undeformed analog of the MSC Sicilian basins?? *Marine and Petroleum Geology*, *124*, 1–20. https://doi.org/10.1016/j.marpetgeo.2020.104777

Réhault, J. P., Honthaas, C., Guennoc, P., Bellon, H., Ruffet, G., Cotten, J., Sosson, M., & Maury, R. C. (2012). Offshore Oligo-Miocene volcanic fields within the Corsica-Liguria Basin: Magmatic diversity and slab evolution in the western Mediterranean Sea. *Journal of Geodynamics*, *58*, 73–95. https://doi.org/10.1016/j.jog.2012.02.003

Rehault, J. P., Mascle, J., & Boillot, G. (1984). Evolution geodynamique de la Mediterrané depuis l'Oligocene. *Bollettino della Società Geologica Italiana*, *27*, 85–96.

Riding, R., Braga, J. C., & Martin, J. M. (1991). Oolite stromatolites and thrombolites, Miocene, Spain: Analogues of Recent giant Bahamian examples. *Sedimentary Geology*, *71*, 121–127. https://doi.org/10.1016/0037-0738(91)90096-V

Roca, E., & Guimerà, J. (1992). The Neogene structure of the eastern Iberian margin: Structural constraints on the crustal evolution of the Valencia trough (western Mediterranean). *Tectonophysics*, *203*, 203–218. https://doi.org/10.1016/0040-1951(92)90224-T

Rosell, L., Orti, F., Kasprzyk, A., Playa, E., & Peryt, T. M. (1998). Strontium geochemistry of Miocene primary gypsum; Messinian of southeastern Spain and Sicily and Badenian of Poland. *Journal of Sedimentary Research*, *68*, 63–79. https://doi.org/10.2110/jsr.68.63

Rosenbaum, G., Lister, G. S., & Duboz, C. (2002). Reconstruction of the tectonic evolution of the western Mediterranean since the Oligocene. *Journal of the Virtual Explorer*, *8*, 107–130. https://doi.org/10.3809/jvirtex.2002.00053

Rouchy, J.-M., & Saint Martin, J.-P. (1992). Late Miocene events in the Mediterranean as recorded by carbonate-evaporite relations. *Geology*, *20*, 629–632. https://doi.org/10.1130/0091-7613(1992)

Roveri, M., Flecker, R., Krijgsman, W., Lofi, J., Lugli, S., Manzi, V., Sierro, F. J., Bertini, A., Camerlenghi, A., De Lange, G., Govers, R., Hilgen, F. J., Hübscher, C., Meijer, P. T., & Stoica, M. (2014). The Messinian Salinity Crisis: Past and future of a great challenge for marine sciences. *Marine Geology*, *352*, 25–58. https://doi.org/10.1016/j.margeo.2014.02.002

Roveri, M., Gennari, R., Lugli, S., & Manzi, V. (2009). The Terminal Carbonate Complex: The record of sea-level changes during the Messinian salinity crisis. *GeoActa*, *8*, 63–77.

Roveri, M., Manzi, V., Bergamasco, A., Falcieri, F. M., Gennari, R., Lugli, S., & Schreiber, B. C. (2014). Dense shelf water cascading and Messinian canyons: A new scenario for the Mediterranean salinity crisis. *American Journal of Science*, *314*, 751–784. https://doi.org/10.2475/05.2014.03

Ryan, W. B. F. (1976). Quantitative evaluation of the depth of the western Mediterranean before, during and after the Late Miocene salinity crisis. *Sedimentology*, *23*, 791–813. https://doi.org/10.1111/j.1365-3091.1976.tb00109.x

Ryan, W. B. F. (2008). Modeling the magnitude and timing of evaporative drawdown during the Messinian salinity crisis. *Stratigraphy*, *5*, 227–243.

Ryan, W. B. F. (2009). Decoding the Mediterranean salinity crisis. *Sedimentology*, *56*, 95–136. https://doi.org/10.1111/j.1365-3091.2008.01031.x

Ryan, W. B. F. (2011). Geodynamic responses to a two-step model of the Messinian salinity crisis. *Bulletin de la Societe Geologique de France*, *182*, 73–78. https://doi.org/10.2113/gssgfbull.182.2.73

Ryan, W. B. F., & Cita, M. B. (1978). The nature and distribution of Messinian erosional surfaces — Indicators of a several-kilometer-deep Mediterranean in the Miocene. *Marine Geology*, *27*, 193–230. https://doi.org/10.1016/0025-3227(78)90032-4

Sàbat, F., Roca, E., Muñoz, J. A., Vergés, J., Santanach, P., Sans, M., Massana, E., Estévez, A., & Santisteban, C. (1997). Role of extension and compression in the evolution of the eastern margin of Iberia: The ESCI-Valencia Trough seismic profile. *Revista de la Sociedad Geológica de España*, *8*, 431–448.

Samperi, L., Giorgio, M., Kamaldeen, O. O., Alba, Z., Nicolas, W., Sabrina, N., Pauselli, C., & Francesco, B. (2020). Estimation of the physical, petrophysical and mineralogical properties of Messinian salt rocks, Sicily: Implications for multidisciplinary applications. *Marine and Petroleum Geology*, *112*, 104032. https://doi.org/10.1016/j.marpetgeo.2019.104032

Schettino, A., & Turco, E. (2006). Plate kinematics of the Western Mediterranean region during the Oligocene and Early Miocene. *Geophysical Journal International*, *166*, 1398–1423. https://doi.org/10.1111/j.1365-246X.2006.02997.x

Sclater, J. G., & Christie, P. A. F. (1980). Continental stretching: An explanation of the post-mid-cretaceous subsidence of the central north sea basin. *Journal of Geophysical Research*, *85*, 3711–3739. https://doi.org/10.1029/JB085iB07p03711

Simon, D., & Meijer, P. T. (2017). Salinity stratification of the Mediterranean Sea during the Messinian crisis: A first model analysis. *Earth and Planetary Science Letters*, *479*, https://doi.org/10.1016/j.epsl.2017.09.045

Speranza, F., Villa, I. M., Sagnotti, L., Florindo, F., Cosentino, D., Cipollari, P., & Mattei, M. (2002). Age of the Corsica-Sardinia rotation and Liguro-Provençal Basin spreading: New paleomagnetic and Ar/Ar evidence. *Tectonophysics*, *347*, 231–251. https://doi.org/10.1016/S0040-1951(02)00031-8

Stein, C. A., & Stein, S. (1992). A model for the global variation in oceanic depth and heat flow with lithospheric age. *Nature*, *359*, 123–129. https://doi.org/10.1038/359123a0

Sternai, P., Caricchi, L., Garcia-Castellanos, D., Jolivet, L., Sheldrake, T. E., & Castelltort, S. (2017). Magmatic pulse driven by sea-level changes associated with the Messinian salinity crisis. *Nature Geoscience*, *10*, 783–787. https://doi.org/10.1038/ngeo3032

Stoica, M., Krijgsman, W., Fortuin, A., & Gliozzi, E. (2016). Paratethyan ostracods in the Spanish Lago-Mare: More evidence for interbasinal exchange at high Mediterranean sea level. *Palaeogeography, Palaeoclimatology, Palaeoecology*, *441*, 854–870. https://doi.org/10.1016/j.palaeo.2015.10.034

Tesauro, M., Kaban, M. K., & Cloetingh, S. A. P. L. (2009). How rigid is Europe's lithosphere? *Geophysical Research Letters*, *36*, 2–7. https://doi.org/10.1029/2009GL039229

Torné, M., Pascal, G., Buhl, P., Watts, A. B., & Mauffret, A. (1992). Crustal and velocity structure of the Valencia trough (western Mediterranean), Part I. A combined refraction/ wide-angle reflection and near-vertical reflection study. *Tectonophysics*, *203*, 1–20. https://doi.org/10.1016/0040-1951(92)90212-O

Urgeles, R., Camerlenghi, A., Garcia-Castellanos, D., De Mol, B., Garcés, M., Vergés, J., Haslam, I., & Hardman, M. (2011). New constraints on the Messinian sealevel drawdown from 3D seismic data of the Ebro Margin, western Mediterranean. *Basin Research*, *23*, 123–145. https://doi.org/10.1111/j.1365-2117.2010.00477.x

Vai, G. B., & Lucchi, F. R. (1977). Algal crusts, autochthonous and clastic gypsum in a cannibalistic evaporite basin: A case history from the Messinian of Northern Apennines. *Sedimentology*, *24*, 211–244. https://doi.org/10.1111/j.1365-3091.1977.tb00255.x

Van Ceuvering, J. A., Berggren, W. A., Drake, R. E., Aguirre, E., & Curtis, G. H. (1976). The terminal Miocene event. *Marine Micropaleontology*, *1*, 263–286. https://doi.org/10.1016/0377-8398(76)90011-6

Vergés, J., & Sàbat, F. (1999). Constraints on the Neogene Mediterranean kinematic evolution along a 1000 km transect from Iberia to Africa. *Geological Society, London, Special Publications*, *156*, 63–80. https://doi.org/10.1144/GSL.SP.1999.156.01.05

Watts, A. B. (2001). *Isostasy and flexure of the lithosphere*. Cambridge University Press.

Watts, A. B., & Ryan, W. B. F. (1976). Flexure of the lithosphere and continental margin basins. *Tectonophysics*, *36*, 25–44.

Watts, A. B., & Torné, M. (1992a). Subsidence history, crustal structure, and thermal evolution of the Valencia Trough: A young extensional basin in the western Mediterranean. *Journal of Geophysical Research*, *97*, 20021. https://doi.org/10.1029/92JB00583

Watts, A. B., & Torné, M. (1992b). Crustal structure and the mechanical properties of extended continental lithosphere in

the Valencia trough (western Mediterranean). *Journal of the Geological Society*, *149*, 813–827. https://doi.org/10.1144/gsjgs.149.5.0813

Watts, A. B., Torné, M., Buhl, P., Mauffret, A., Pascal, G., & Pinet, B. (1990). Evidence for reflectors in the lower continental crust before rifting in the Valencia trough. *Nature*, *348*, 631–635. https://doi.org/10.1038/348631a0

Watts, A. B., Zhong, S. J., & Hunter, J. (2013). The Behavior of the Lithosphere on Seismic to Geologic Timescales. *Annual Review of Earth and Planetary Sciences*, *41*, 443–468. https://doi.org/10.1146/annurev-earth-042711-105457

Wessel, P., Smith, W. H. F., Scharroo, R., Luis, J., & Wobbe, F. (2013). Generic mapping tools: Improved version released. *Eos, Transactions American Geophysical*, *94*, 409–410. https://doi.org/10.1002/2013EO450001

Yelles, A., Domzig, A., Déverchère, J., Bracène, R., Mercier de Lépinay, B., Strzerzynski, P., Bertrand, G., Boudiaf, A., Winter, T., Kherroubi, A., Le Roy, P., & Djellit, H. (2009). Plio-Quaternary reactivation of the Neogene margin off NW Algiers, Algeria: The Khayr al Din bank. *Tectonophysics*, *475*, 98–116. https://doi.org/10.1016/j.tecto.2008.11.030

Yoshimura, T., Kuroda, J., Lugli, S., Tamenori, Y., Ogawa, N. O., Jiménez-Espejo, F. J., Isaji, Y., Roveri, M., Manzi, V., Kawahata, H., & Ohkouchi, N. (2016). An X-ray spectroscopic perspective on Messinian evaporite from Sicily: Sedimentary fabrics, element distributions, and chemical environments of S and Mg. *Geochemistry, Geophysics, Geosystems*, *17*, 1383–1400. https://doi.org/10.1002/2015GC006233

**How to cite this article:** Heida, H., Raad, F., Garcia-Castellanos, D., Jiménez-Munt, I., Maillard, A., & Lofi, J. (2021). Flexural-isostatic reconstruction of the Western Mediterranean during the Messinian Salinity Crisis: Implications for water level and basin connectivity. *Basin Research*, 00, 1–31. https://doi.org/10.1111/bre.12610

## APPENDIX A
## LOCAL ISOSTASY CALCULATION

Deflection sediment units:

$$\left(h_s - w\right) \times \rho_w + d \times \rho_m = h_s \times \rho_s \tag{A1}$$

$$w \times \rho_m - d \times \rho_w = h_s \times \rho_s - h_s \times \rho_w \tag{A2}$$

$$w \times \left(\rho_m - \rho_w\right) = h_s \times \left(\rho_s - \rho_w\right) \tag{A3}$$

$$w = h_s \times \frac{\left(\rho_s - \rho_w\right)}{\left(\rho_m - \rho_w\right)} \tag{A4}$$

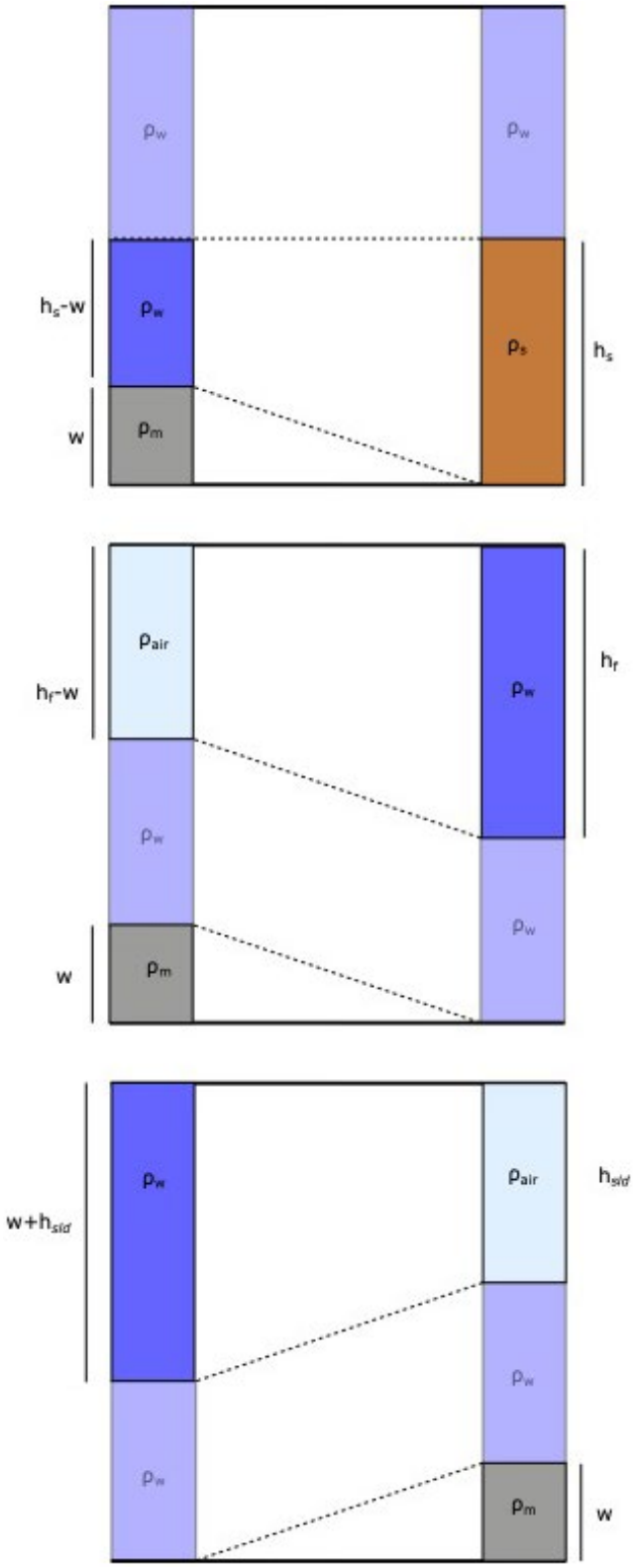


Deflection flood:

$$h_f \times \rho_w = w \times \rho_m + \left(h_f - w\right) \times \rho_{air} \tag{A5}$$

$$w = h_f \times \frac{\rho_w}{\rho_m} \tag{A6}$$

Deflection Sea-level drop:

$$h_{sld} \times \rho_w + d \times \rho_w = h_{sld} \times \rho_{air} + w \times \rho_m \quad \text{(A7)}$$

$$w \times (\rho_a - \rho_w) = h_{sld} \times \rho_w \quad \text{(A8)}$$

$$w = h_{sld} \times \frac{\rho_w}{(\rho_m - \rho_w)} \quad \text{(A9)}$$

where $w$ is the magnitude of deflection; $\rho_w$ = water density (1,030 kg/m$^3$); $\rho_m$ = mantle density (3,250 kg/m$^3$); $\rho_{air}$ = air density (0 kg/m$^3$); $\rho_s$ = sediment density (see Table 1); $h_s$ = sediment thickness; $h_{sld}$ is the magnitude of water level drop; $h_f$ is the magnitude of change in water level during flooding.

Load versus deflection ratio for each modelling step under local isostasy

| Unit | Equation | Ratio $w/h$ |
|---|---|---|
| MU | $w = h_s \times \frac{\rho_s - \rho_w}{\rho_a - \rho_w}$ | 0.51 |
| UU | $w = h_s \times \frac{\rho_s - \rho_w}{\rho_a - \rho_w}$ | 0.66 |
| PQ | $w = h_s \times \frac{\rho_s - \rho_w}{\rho_a - \rho_w}$ | 0.48 |
| Flooding | $w = h_f \times \frac{\rho_w}{\rho_a}$ | 0.317 |
| Sea-level drop | $w = h_{sld} \times \frac{\rho_w}{\rho_a - \rho_w}$ | 0.46 |

*Note:* Relationship between load thickness ($h$) and deflection ($w$) for each step of the backstripping. For sedimentation steps, we assume sediments are replacing water. Variable names are same as above.

## APPENDIX B

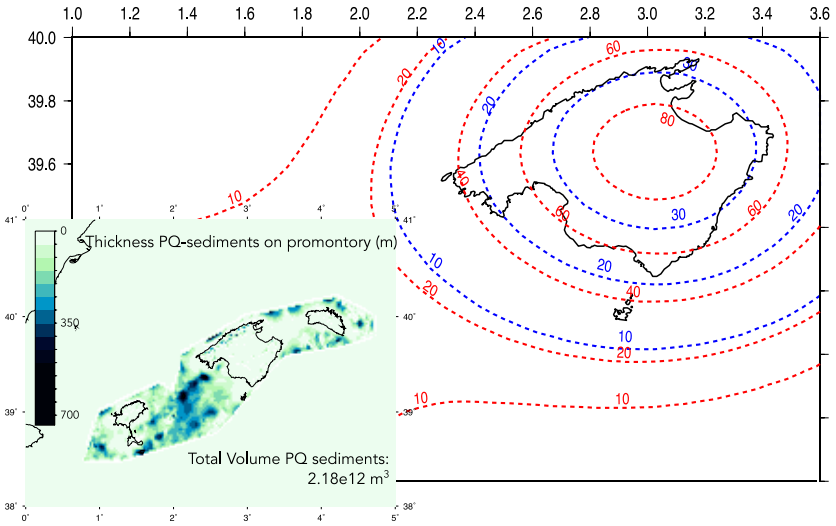


Thickness map of PQ sediments on the Balearic promontory and isolines for flexural-isostatic rebound effect in m for a range of post-Messinian erosion values based on 30%–70% clastic provenance sediments on Balearic Promontory. Blue: minimum volume clastics (0.65e12 m3, corresponding to the 30% clastic component limit and implying an average 133 m of erosion onland) Red: maximum volume clastics (1.52e12 m3, corresponding to the 70% clastic component limit and implying an average 310 m of erosion onland). Rebound calculated for EET value of 15 km.